UNIVERSITÀ DEGLI STUDI DI PADOVA

Dipartimento di Fisica e Astronomia "Galileo Galilei"

Corso di Laurea in Fisica

Tesi di Laurea

Optimal three-qubit gates with Rydberg atoms

Porte logiche quantistiche ottimali a tre qubit con atomi di Rydberg

Relatore

Dr. Pietro Silvi

Correlatore

Prof. Simone Montangero

Laureando

Giovanni Concheri

Anno Accademico 2022/2023

Contents

Abstract

Making use of sophisticated physical systems such as Rydberg atoms, it is possible to implement controllable quantum many-body systems, giving access to the realization of more and more powerful quantum computers in the pursuit of quantum supremacy, one of the main goals of quantum computing. Thanks to these atoms' peculiar characteristics, such as having a high principal quantum number along with other exaggerated properties, it is possible to realize quantum gates that require interaction between two qubits such as the "controlled-phase" gate. The research here presented aims to go one step further in the study of the interaction between qubits in Rydberg atoms, analyzing the realization of a three-qubit quantum logic gate with Rydberg atoms called a "controlled-controlled-phase" (flip) gate. In the first part, the project aims to test whether the conditions for the actual realization of the gate are met. In particular, with the use of GNU Octave scripts, firstly we check if the Hamiltonian operators have complete control over the unitary operators that are invariant for permutations of two qubits out of three. Secondly, we verify that the c-c-phase gate belongs to the closed Lie algebra of these Hamiltonian operators. Finally, in the second part, with the use of sophisticated Quantum Optimal Control algorithms (QuOCS), we attempt to obtain the actual optimization of this gate.

Facendo uso di sofisticati sistemi fisici realizzati con atomi di Rydberg, è possibile implementare sistemi quantistici controllabili a molti corpi, dando così accesso alla realizzazione di computer quantistici sempre più potenti nell'incessante tentativo di raggiungere la "supremazia quantistica", uno degli obiettivi principali del campo di ricerca della computazione quantistica. Grazie al numero quantico principale molto alto di questi atomi e grazie ad altre loro proprietà esagerate, è possibile realizzare porte logiche quantistiche che necessitano di interazione tra due qubit come, ad esempio, il "controlled-phase" gate. Questa ricerca mira a fare un ulteriore passo in avanti nello studio dell'interazione di qubit negli atomi di Rydberg, andando ad analizzare l'implementazione di una porta logica quantistica a 3 qubit con atomi di Rydberg, nota come "controlled-controlled- phase" (flip) gate. Nella prima parte, il progetto ha come obiettivo quello di controllare che le condizioni necessarie per la realizzazione della porta logica siano effettivamente verificate. In particolare, con l'utilizzo di codici scritti su GNU Octave, verifichiamo innanzitutto che gli operatori Hamiltoniani abbiano completo controllo sugli operatori unitari invarianti per permutazioni di due qubit sui tre a disposizione. Successivamente, verifichiamo che il "c-c-phase" gate appartenga alla chiusura dell'algebra di Lie degli operatori Hamiltoniani. Nella seconda parte, facendo uso di sofisticati algoritmi di Quantum Optimal Control (QuOCS), tentiamo infine di realizzare l'effettiva ottimizzazione della porta logica.

Chapter 1

Introduction

"Let the computer itself be built of quantum mechanical elements which obey quantum mechanical laws." This is what the physicist Richard Feynman stated in 1982, considering the idea that a quantum device could take advantage of purely quantum phenomena such as superposition and entanglement to better describe the intrinsically quantum nature of the physical world [1].

This simple yet groundbreaking concept marked the birth of two incredibly innovative research areas known as quantum simulation and quantum computing. The first consists of using a quantum system to model the behavior of another one, while the latter seeks to solve numerical problems by making use of quantum circuits, which consist of a network of quantum logic gates, that are the basic building blocks of quantum algorithms. These gates perform specific operations manipulating the information stored in two-level systems, known as qubits, that are the quantum version of the classical bits [2].

Quantum computers, by exploiting the unique features of quantum mechanics, have the potential to solve certain problems exponentially faster than any classical computer. This feat, known as quantum supremacy, has not yet been achieved, but there has been considerable progress towards its accomplishment [3]. Its achievement would indeed revolutionize fields such as cryptography [4], condensed-matter physics [5] and industrial applications, holding tremendous promise for solving some of the most challenging problems in science and technology.

Over the past few decades, various quantum devices have been developed. Among the most common ones we find superconducting loops [6], trapped ions [7], and neutral atoms [2], where an effective two-level system has been implemented.

Of these methods, neutral atoms have several attractive features that make them a promising system for quantum computing, especially for their high scalability to large numbers of qubits, opening the door to multi-qubit quantum processing and taking a step closer to quantum supremacy. This is due to the fact that they interact weakly and therefore can be packed closely to each other.

In addition, these atoms can be readily prepared by optical pumping in well-defined initial states that in some cases can be well isolated from the environment, allowing for long decoherence times, an essential feature for high-fidelity quantum computing. Most notably, qubit states encoded in neutral atoms can be rapidly and accurately controlled with electromagnetic fields, thus permitting the realization of quantum gates obtained by making use of laser beams that are tightly focused on individual atoms trapped in optical tweezers to drive atomic transitions between hyperfine levels [8, 2].

To have a complete set of quantum operations at our disposal, entangling gates are required, and given the weak interaction taking place between neutral atoms, a solution is to temporarily excite them to Rydberg atoms [9]. These atoms, initially studied by Johannes Rydberg at the end of the 1800s, have attracted significant attention in the field of quantum computing due to their exaggerated properties such as having a very high quantum principal number and a large electric dipole moment. In fact, atoms excited to the Rydberg state strongly interact with dipole-dipole interaction enabling a phenomenon known as Rydberg Blockade, that quenches the simultaneous excitation of nearby Rydberg atoms on distances up to several micrometers [10]. This effect leads to entanglement of qubits and is an effect of crucial importance for the implementation of entangling gates. The idea of making use of the strong interaction between Rydberg atoms to realize entangling quantum gates was first suggested at the end

of the 1990s [9]. After several years, in 2009 the first experimental demonstrations of Rydberg Blockade were carried out [11, 12], leading to a boost in research aiming to the realization of entangling gates with Rydberg atoms. In 2019, it has been shown how to implement a controlled-phase gate with a Bell-state fidelity greater than 97.4% with Rubidium-87 atoms [13]. In addition, theoretical results have demonstrated that a Bell-state fidelity greater than 99.9% is achievable on a Strontium-88 platform [10], showing how the fidelity of Rydberg atoms is now just as competitive as the one of other quantum devices such as trapped ions. Furthermore, theorical research is also aiming to extend these ideas to multiqubit gates [14], in particular three-qubit gates, namely the main focus of this project.

The three-bit gate was first introduced by Tommaso Toffoli in 1980, with the classical Toffoli (CCNOT) gate, which was then easily translated into the quantum logic version that consists of a doubly-controlled NOT gate where the state of the target qubit changes depending on the state of the two control qubits. Research on three-qubit gates highlighted several attracting properties of these gates. For instance, we only have to consider one single-qubit gate along with the Toffoli one to form a universal set of quantum gates [15]. Furthermore, the Toffoli gate is a key element for faster implementation of algorithms such as quantum error correction schemes [16, 17].

Most notably, by using Toffoli gates, we are significantly reducing the time duration of these computation processes. Since the dominant source of error in the implementation of a Rydberg quantum gate is the decay rate of the Rydberg state [10] reducing the time spent in the Rydberg state is another crucial advancement we want to make to enhance the gate's fidelity. That is why in this Thesis we aim to realize a three-qubit gate known as the "controlled-controlled-phase gate" by making use of Quantum Optimal Control Algorithms in Python (QuOCS) [18].

This Thesis is structured as follows:

- In Chapter 2, firstly we introduce the Rydberg atoms by examining their main properties. Secondly, we give a rigorous analysis of the qubit and of the quantum gates, focusing in particular on the two-qubit controlled-phase gate. Finally, we introduce the three-qubit gates by further examining their advantages in quantum computing.

- In Chapter 3, we test whether the conditions for the actual realization of the controlled-controlled-phase gate are met. We start by describing the setup of the Rydberg system with which we want to create the gate. Then, with the use of GNU Octave scripts, we check if the Hamiltonian operators have complete controllability over the unitary operators that are invariant for permutations of two qubits out of three. Consequently, we check that the c-c-phase gate belongs to the closed Lie algebra of these Hamiltonian operators. Finally, we verify which time-dependent parameters of the laser pulse are negligible in sight of its optimization for the implementation of the c-c-phase gate.

- In Chapter 4, we proceed with the actual optimization of the laser pulse. We firstly give a brief introduction on the Quantum Optimal Control Theory (QOCT), by outlining the main Quantum Optimal Control (QOC) problem, then applying it to our specific setup. Secondly, we give a brief explanation of the dCRAB algorithm that resolves the control problem. We then explain the main conceptual passages made to adapt the algorithm to our specific case. Finally, we outline the optimization settings and the results consequently obtained.

Chapter 2

Quantum Computing with Neutral Atoms

Neutral atoms have several enticing features that make them an ideal candidate for quantum computing, most of which are related to their high scalability to large numbers of qubits. To name a few, the atoms are all identical and can readily be prepared by optical pumping in well-defined initial states. Their qubit states can be precisely measured using fluorescence, and in some cases they can be well isolated from the environment, which allows for long decoherence times. In addition, they can be trapped in close proximity since the interaction between them is weak. Most importantly, the qubit states can be rapidly and accurately controlled with electromagnetic fields [8, 2]. Thus, quantum gates can be obtained with Rydberg atoms.

The main idea behind a quantum Rydberg gate is to trap the neutral atoms with optical tweezers in a 2-dimensional lattice and then make use of laser beams that are tightly focused on individual atoms to drive atomic transitions between hyperfine levels. Another way is to drive atomic transitions with more easily controlled microwaves [2].

In particular, to implement entangling gates strong interactions among qubits are required. Given the weak interaction between neutral atoms, a solution is to temporarily excite atoms to Rydberg states. In this way, the atoms enable a phenomenon called Rydberg Blockade which can be used to entangle qubits. This phenomenon is described in depth in the following section (Sec. 2.1).

After the first experimental demonstrations of Rydberg Blockade [11, 12], a large theoretical interest is focused on the two-qubit controlled-phase gate, endeavoring to improve the gate fidelity, showing that an average gate fidelity above 99.9% is achievable [10]. Furthermore, theorical research is also aiming to extend these ideas to multiqubit gates [14] which is what we are going to focus on, examining a specific three-qubit gate, the controlled-controlled-phase gate.

In section 2.1 we introduce the Rydberg atoms by examining their main properties. In section 2.2 we rigorously introduce the concept of qubit along with quantum gates, exploring how they work by specifically analyzing the controlled-phase gate analyzed in Ref. [10]. We then finally introduce the three-qubit gates and examine the advantages they offer in quantum computing.

2.1 Rydberg Atoms

Rydberg atoms are excited atoms with one or more electrons in a highly excited state, with principal quantum number $n \geq 10$ [1]. In such conditions, the atoms' diameter is of the order of micrometers, approximately a factor 10^4 larger than that of a neutral atom in the ground state. Their massive size leads them to exhibit several exaggerated properties which are incredibly useful for quantum computation.

In fact, since both their size and their electric dipole moment scale as n^2 they present huge dipole matrix elements, which lead to strong interactions between atoms. This strong interaction enables a phenomenon called Rydberg blockade. This effect prevents the simultaneous excitation to a specific Rydberg state of nearby Rydberg atoms on distances up to a few micrometers and can be exploited to entangle several qubits [19]. In addition, this implies that the Rydberg atom is very sensitive to

[1] I.e. The Rydberg state for the Strontium-88 Rydberg atom presented in Ref. [10] has n = 60.

external electromagnetic fields, making it ideal for the creation of a quantum gate by controlling its dynamics with specific laser pulses.

Furthermore, Rydberg atoms have arguably long decoherence times, that scale as n^3. Finally, another great advantage of neutral atoms is that on distances greater than a few micrometers the interaction between atoms becomes very weak and the Rydberg blockade is essentially absent, permitting us to pack a lot of atoms close to each other, paving the way for multiqubit quantum computing.

In Section 2.1.1 we describe more rigorously the decoherence time along with other properties of the Rydberg atoms. In Section 2.1.2 we describe the interaction between Rydberg atoms and finally explore the Rydberg Blockade mechanism.

2.1.1 Main properties

To simplify the approach, we can treat the Rydberg atoms as hydrogenic, and by calculating the orbit size we see that it actually scales as n^2. Now, let us first briefly examine the lifetime of Rydberg atoms. Since they are in an excited state, they are naturally unstable and they decay with a characteristic lifetime τ, that varies depending on the Rydberg state, eventually falling to the ground state. The decay is governed by two main physical processes: one is spontaneous emission caused by perturbation of the vacuum electromagnetic fluctuations at 0 K. Its rate defines the radiative lifetime τ_0 of the atom. The other is stimulated emission caused by blackbody radiation (BBR) at finite temperature T with a rate τ_{bb} [19]. The total lifetime of the Rydberg atom is defined as:

$$\frac{1}{\tau} = \frac{1}{\tau_0} + \frac{1}{\tau_{bb}} \tag{2.1}$$

Focusing on the radiative lifetime, with rigorous analysis we can show that it scales with n^3 for transitions to low-energy states, and with n^5 for those to neighbouring Rydberg states. The transitions to low-lying states constitute dominant channels of spontaneous emission, so the radiative life-time is approximately proportional to n^3 [19]. By the results obtained in Ref. [10], where different error contributions were considered in the calculation of the fidelity of a controlled-phase gate, the Rydberg state decay is what turns out to be the dominant source of error. In particular, it corresponds to 90% of the total error, given by the sum of three contributions: the finite lifetime of the Rydberg level, the recoil of the single-photon transition and the force experienced by the atoms due to van der Waals interaction, the last two being motional cooling errors. This implies that minimization of the time duration of the gate plays a role of crucial importance to do effective quantum computing with neutral atoms.

2.1.2 Interaction Between Rydberg Atoms

Now let us consider two neutral atoms, each having an electron in the Rydberg state, separated by a distance R. Assuming R to be much greater than the size of the electronic wave-function, we can limit ourselves to consider the electrostatic interaction between two charge distributions using the electric multipole expansion in spherical coordinates [8, 20]. In this case, the interaction reduces to dipole-dipole interaction as other interactions can be neglected. Recalling the definition of the dipole moment operator $\mathbf{p} = -e\mathbf{d}$, the interaction can be expressed as:

$$\mathrm{V}_{dd} = \frac{e^2}{4\pi\epsilon_0} \frac{\mathbf{d}_1 \cdot \mathbf{d}_2 - 3(\mathbf{d}_1 \cdot \hat{\mathbf{e}}_R)(\mathbf{d}_2 \cdot \hat{\mathbf{e}}_R)}{|\mathbf{R}|^3} \ , \tag{2.2}$$

where $\hat{\mathbf{e}}_R$ is the unit vector along the relative coordinate R between two atoms, and $\mathrm{R} = |\mathbf{R}|$ is the separation between the atoms [See Figure 2.1a]. Such dipolar interaction scales as $V_{dd} \propto n^4$ because the dipole moment scales as $|\mathbf{d}| \propto n^2$.

Therefore, if the system of two non-interacting Rydberg atoms can be described by a static Hamiltonian H_0, considering the dipole-dipole interaction the Hamiltonian now becomes:

$$\mathrm{H} = \mathrm{H}_0 + \mathrm{V}_{dd} \tag{2.3}$$

Because of this interaction, we know from perturbation theory that the eigenstate $|rr\rangle$ of the static Hamiltonian which describes the outer electrons experiences an energy shift ΔE with the respect to its bare energy E_{rr}. We now want to calculate the energy shift.

To accomplish this, let us first notice that:

$$\langle \mathbf{d}_{nlm} \rangle := \langle \Psi_{nlm} | \mathbf{d}(t) | \Psi_{nlm} \rangle \xrightarrow{|\Psi_{nlm}\rangle = |rr\rangle} \langle \mathbf{d}_{nlm} \rangle = \langle rr | \mathbf{d}(t) | rr \rangle = 0 \tag{2.4}$$

In words, the spatial symmetry of the wave-functions $|\Psi_{nml}\rangle$ results in a vanishing static dipole moment, which therefore implies that $\langle \mathrm{V}_{dd} \rangle = 0$. On the contrary, the dipole matrix elements between eigenstates with different parities are instead non-zero, and we can demonstrate that in the case of a single transition from $|rr\rangle$ to $|r_1' r_2'\rangle$, where $|r_1'\rangle$ $|r_2'\rangle$ are different Rydberg states, we can describe the system restricting ourselves to the subspace $\{|rr\rangle, |r_1' r_2'\rangle\}$, and by defining the Hamiltonian

$$\hat{H} = \begin{bmatrix} 0 & C_3/R^3 \\ C_3/R^3 & \delta_F \end{bmatrix} , \tag{2.5}$$

where $C_3 \propto n^4$ is the anisotropic interaction coefficient and $\delta_F = (E_{r_1'} + E_{r_2'}) - (E_r + E_r)$ the Foster defect defined as the difference of the bare energy between final and initial pair states [19]. Let us take note that the non-diagonal matrix elements which represent the dipole-dipole interaction that couple the state $|rr\rangle$ with $|r_1' r_2'\rangle$ are proportional to R^{-3}.

We now restrict to the case where $\delta_F \gg V(R) := C_3/R^3$, which is the regime where we can calculate the energy shift as a perturbative correction. The calculation of the first order energy correction is given by the dipole-dipole interaction expectation value $\langle \mathrm{V}_{dd} \rangle$, which corresponds to the first element of the matrix in Eq. (2.5). We notice that it is zero, as also concluded in Eq. (2.4). We thus consider the second-order perturbative correction, which is defined as:

$$\Delta E = \mathrm{E}_{rr}^{(2)} = \sum_{|r_1' r_2'\rangle} \frac{|\langle r_1' r_2' | V_{dd} | rr \rangle|^2}{2E_r - E_{r_1'} - E_{r_2'}} = \frac{C_{6,rr}}{R^6} . \tag{2.6}$$

This interaction is conventionally called van der Waals interaction [21, 22] with $C_{6,rr}$ the van der Waals coefficient, which scales with n^{11}. We will consider this as the Rydberg-Rydberg interaction in the next chapters.

We can now acknowledge two of the main properties of Rybderg atoms outlined at the beginning of the Chapter. On one hand, the strong interactions between adjacent or nearby atoms placed in an optical lattice, highlighted by the fact that the $C_{6,rr}$ coefficient scales with n^{11}. On the other hand, the weak interactions between non-adjacent Rydberg atoms, being $V \propto 1/R^6$ and therefore dropping quickly to small values as the distance between atoms increases (R of a few micrometers).

We now want to study how the strong interaction between Rydberg atoms activates the Rydberg blockade effect. Let us consider a system of two atoms, each having a ground state $|g\rangle$ and a Rydberg state $|r\rangle$. Let us now activate a resonant laser field that couples the ground state $|g\rangle$ to $|r\rangle$ with Rabi frequency Ω[2].

If we now describe the system in a basis given by vector states $\{|gg\rangle, |+\rangle = \frac{|gr\rangle + |rg\rangle}{\sqrt{2}}, |-\rangle = \frac{|gr\rangle - |rg\rangle}{\sqrt{2}}, |rr\rangle\}$ we find that the states $|gg\rangle$ and $|+\rangle$ are coupled with Rabi frequency $\sqrt{2}\Omega$, whereas $|+\rangle$ and $|rr\rangle$ are not [8].

In fact, in Eq. 2.6 we derived that the strong mutual interaction between Rydberg atoms induces an energy shift in the state $|rr\rangle$, and this implies that the resonant frequency we would need to excite the state $|+\rangle$ to $|rr\rangle$ is greater than the one of the laser, since the difference in energy between these states is greater than the one between $|gg\rangle$ and $|+\rangle$. This conclusion is valid when $C_6/R^6 \gg \hbar\Omega$, which denotes the regime of strong interaction. We can rewrite it as $R_b \gg R$ where $R_b = (C_6/\hbar\Omega)^{1/6}$ is the blockade radius [8].

A question we could raise is: why does the interaction not perturb the energies of $|gg\rangle$ and $|+\rangle$? This is due to the fact that there is very little dipole-dipole interaction between two ground states and

[2]The Rabi frequency defines the frequency at which the probability amplitudes of two atomic energy levels fluctuate in an oscillating electromagnetic field [23]

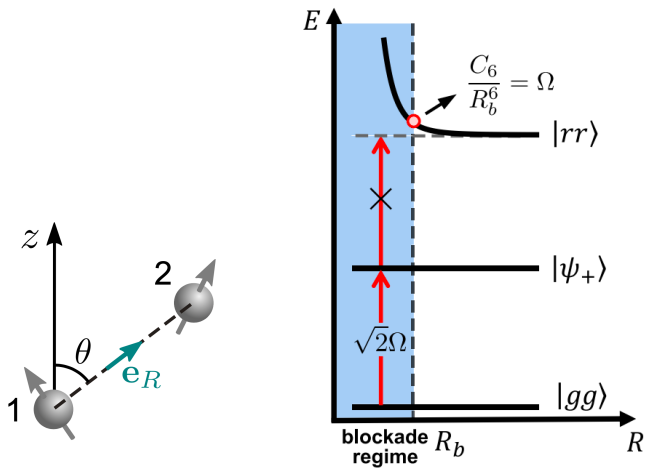

(a) (b)

Figure 2.1: *Rydberg interaction and Rydberg blockade. (a) Dipole-dipole interaction between two atoms with interatomic separation R to the quantization axis z. (b) Rydberg blockade in the two-atom case. Figures from Ref. [19]*

between a ground state and a Rydberg one. In fact the dipole interaction in the latter cases is at least 11 orders of magnitude smaller than the one between two Rydberg states, since the interaction scales with n^{11} and the principal quantum number of Ryderg states is around 10 times the one of the ground state. Therefore, the perturbative correction in these cases is considered to be negligible. As a result, in the regime of strong interaction the laser couples $|gg\rangle$ and $|+\rangle$, and it is instead off-resonant with the energy transition between $|+\rangle$ and $|rr\rangle$, meaning that the state $|rr\rangle$ is decoupled [see Fig. 2.1b]. This implies that one cannot excite two atoms simultaneously to Rydberg states if they are located sufficiently close-by to each other. This effect is called Rydberg blockade.[3]

With no exaggeration, we can state that this phenomenon is the backbone of quantum computing with Rydberg atoms, as it enables the entanglement of qubits, hence the creation of entangling quantum logic gate, such as the controlled-phase gate examined in Ref. [10] and also the gate we are aiming to realize, the controlled-controlled-phase gate.

To conclude, let us notice that the dipole-dipole interaction between atoms that are in the Rydberg state is an effect that can neither be manipulated nor "shut down". Therefore we cannot control the Rydberg state and its dynamics, thus indicating our inability to use them as computational states. What we can and will do is use them as states of support in order to enable quantum entanglement[4].

Another reason why we cannot use $|r\rangle$ as a computational state is because the Rydberg state decades rapidly with respect to the qubit states that present long decoherence times. This also implies that in the optimization of the gate we should also minimize its time duration, finding the minimum time for the gate to couple the state without, therefore limiting the error introduced by the Rydberg decay (see Subsection 2.1.1).

2.2 Quantum Gates

2.2.1 Quantum computing with qubits

A qubit (quantum bit) is a basic unit of quantum information, that is the quantum version of the classic binary bit. It is a two-level quantum system where the two basis qubit states are denoted as $|0\rangle$ and $|1\rangle$ [24]. Generally, a pure qubit state is a unit vector in a two-dimensional Hilbert space and

[3]Let us notice that what we have concluded is valid in the regime of perfect Rydberg Blockade, where the van der Waals interaction strength $V = C_6/R^6$ is infinite. In reality, even though $V \gg \hbar\Omega$, V is finite and this leads to a very small probability of both atoms being excited to the Rydberg state.

[4]Entanglement is a phenomenon that entails an intrinsic correlation between the constituents of a quantum system.

can be written as a linear combination, or coherent superposition, of the basis states:

$$|\Psi\rangle = \alpha\,|0\rangle + \beta\,|1\rangle \tag{2.7}$$

where $\alpha, \beta \in \mathbb{C}$ are probability amplitudes with the constraint $|\alpha|^2 + |\beta|^2 = 1$.

Examples of quantum systems that have two distinguishable states are the electron spin, where the two levels are usually referred to as "spin up" and "spin down", and the polarization of a single photon, which can be measured as either "vertical polarization" or "horizontal polarization". In the case of neutral atoms, the qubits are encoded in two hyperfine states of the atoms [2], which we refer to as $|0\rangle$, ground state, and $|1\rangle$, excited state, together named computational states. As outlined at the beginning of the chapter, we know this to be an efficient system to encode a qubit since these states can be well isolated from the environment, which allows for long decoherence times. To complete the quantum system that underlies Rydberg qubits we also have to consider another state, which is the Rydberg state $|r\rangle$ (support state)[5]. As concluded in Subsection 2.1.2, it is in fact essential for entanglement. Therefore, we assume the Rydberg qubit to be a three-level system, consisting of $|0\rangle$, $|1\rangle$ and $|r\rangle$.

The last thing we want to outline about the qubit is that by operating a suitable change of coordinates and exploiting the undetectability of global phases in quantum mechanics, the qubit state can be rewritten as:

$$\frac{\cos\theta}{2}\,|0\rangle + e^{i\phi}\frac{\sin\theta}{2}\,|1\rangle \tag{2.8}$$

where $0 \leq \theta \leq \pi$ and $0 \leq \phi \leq 2\pi$. Thus, we can describe the qubit state as a point on a three-dimensional unitary sphere, called Bloch sphere.

Having introduced the concept of qubit we can now have a better idea of what quantum computing actually is. In a nutshell, it consists of acting on a qubit register by means of a quantum algorithm. By applying the quantum circuit model, we can represent algorithms as a sequence of quantum gates performed on one or more qubits [8]. Here, an N-qubit quantum gate is an operation that is applied on N qubits changing their quantum state. It can be represented by a unitary operator (matrix) of dimension $2^N \times 2^N$. Since they are unitary, any single-qubit gate corresponds to a rotation of the state vector onto the Bloch sphere.

In the specific case of Rydberg quantum gates, single-qubit gates are performed with laser beams that couple the ground state $|0\rangle$ and the excited state $|1\rangle$. Let us now briefly outline the physics of these gates. We consider a laser described by an oscillating electric field, e.g. a monochromatic plane wave $\mathbf{E}(t) = \mathbf{E}_0\cos(\omega t + \phi)$, with angular frequency ω and phase ϕ . To simplify the approach, we neglect the spatial term of the laser as if we were studying the system in a fixed point. The interaction between the atom and the field can be reduced to:

$$\hat{H}_{int} = -\mathbf{p}\cdot\mathbf{E}(t)\ , \tag{2.9}$$

where $\mathbf{p}$ is the electric dipole of the atom.

Now, we describe the Hamiltonian of the system in analogy with Eq. (2.3) as $\hat{H} = H_0 + H_{int}$ where H_0 is the static Hamiltonian of the Rydberg atom, and H_{int} is the interaction defined in Eq. (2.9). Thus, we obtain:

$$\hat{H} = \hbar\omega_0\,|0\rangle\langle 0| + \hbar\omega_1\,|1\rangle\langle 1| + \hbar\Omega\cos(\omega t + \phi)(|1\rangle\langle 0| + |0\rangle\langle 1|)\,, \tag{2.10}$$

where we have introduced the Rabi frequency which can now be defined rigorously as $\Omega = \mathbf{p}\cdot\mathbf{E}_0/\hbar$ [8]. Now by applying the rotating wave approximation, where we assume $\Delta, \Omega \ll \omega$, and rewriting the Hamiltonian within the rotating frame of reference[6] we obtain the final form of the Hamiltonian:

$$\hat{H} = -\hbar\frac{\Delta}{2}\,|0\rangle\langle 0| + \hbar\frac{\Delta}{2}\,|1\rangle\langle 1| + \hbar\frac{\Omega}{2}(|1\rangle\langle 0| + |0\rangle\langle 1|) \tag{2.11}$$

where we have defined the detuning of the laser relative to the transition frequency as $\Delta = \omega_1 - \omega_0 - \omega$ [25]. In words, the laser detuning defines the difference between the laser's optical frequency and the atomic transition resonance frequency [26].

[5] We may even want to consider more than one Rydberg state in the encoding of a qubit, as they may be useful to make measurements

[6] For more details see Ref. [8]

2.2.2 The controlled-phase gate

To do quantum computing, we need a universal quantum computing gate set, which is a set of gates to which any operation possible on a quantum computer can be reduced. To obtain this, we must introduce entangling operations in addition to an arbitrary single-qubit gate. For instance, we can achieve this by making use of the two-qubit controlled-phase gate along with a set of generators for single-qubit gates [27]. It has been demonstrated that this gate, also known as CZ gate, can be implemented by making use of the Rydberg Blockade [11, 12], as anticipated in Subsection 2.1.2 where we acknowledged the vital importance of this phenomenon for entangling gates.

Let us now briefly describe the controlled-phase gate presented in Ref. [10]. We consider two Rydberg qubits with states $|0\rangle$ and $|1\rangle$ and the Rydberg state $|r\rangle$ encoded into two Rydberg atoms, and a global laser homogeneously driven on the Rydberg atoms. The state $|r\rangle$ is coupled with $|1\rangle$ by means of the laser electromagnetic field with Rabi frequency $\Omega(t)$ and detuning $\Delta(t)$, in analogy with the coupling of $|0\rangle$ and $|1\rangle$ in the single-qubit gate analyzed in Eq. (2.11). In addition, we have derived that two Rydberg atoms interact with dipole-dipole interaction shifting the energy of the $|rr\rangle$ state (sse Subsec. 2.1.2). The interaction strength is quantified by $V = C_6/R^6$ and since we want to exploit the Rydberg blockade effect for entangling we must assign a value to V for which $V/\hbar\Omega \gg 1$. Overall, the Hamiltonian of the system is given by

$$\mathrm{H} = \mathrm{H}_0 + \mathrm{H}_{int} \ , \tag{2.12}$$

where the first term, H_0 accounts for the coupling to the Rydberg state by means of the laser field, within the rotating frame and applying the rotating wave approximation. The second term H_{int} accounts for the dipole-dipole interaction:

$$\mathrm{H}_0 = \hbar \sum_{i=1}^{2} \left[\frac{\Omega(t)}{2} |r\rangle\langle 1|_i + |1\rangle\langle r|_i - \Delta(t) |r\rangle\langle r|_i \right] \ ; \ \mathrm{H}_{int} = -\frac{C_6}{R^6} |rr\rangle\langle rr| \tag{2.13}$$

Since $|0\rangle$ is uncoupled by the laser, it does not evolve, therefore the gate trivially maps $|00\rangle$ in $|00\rangle$. At this point, the dynamics of $|01\rangle$ can be described in a two-level system $\{|01\rangle, |1r\rangle\}$ with Rabi frequency Ω_0. The same applies for $|10\rangle$, being the setup symmetric. Instead, as seen in Subsec. 2.1.2, the dynamics of $|11\rangle$ follows a two-level system composed by $\{|11\rangle, \frac{|1r\rangle + |r1\rangle}{\sqrt{2}}\}$ with an enhanced Rabi frequency $\sqrt{2}\Omega_0$. The different Rabi frequency for the two states $|01\rangle$ and $|11\rangle$ leads to different trajectories of the states on the Bloch sphere [see Figure 2.2] and, therefore, the state $|11\rangle$ picks up a phase ϕ_{11} which is different from the phase $\phi_{01} = \phi_{10}$ picked up by $|10\rangle$ and $|01\rangle$ [10]. Finally, if we require that the phases satisfy the relation given by

$$\phi_{11} = 2\phi_{01} + \pi \ , \tag{2.14}$$

we realize a controlled-phase gate, up to a global rotation by ϕ_{01} of the excited state $|1\rangle$.

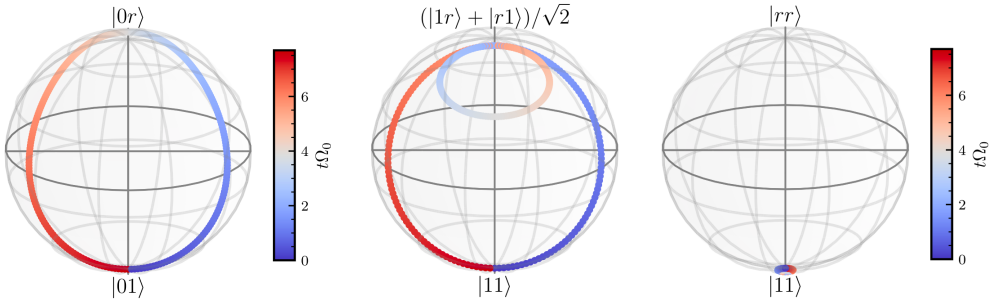

(a) (b)

Figure 2.2: *Non-trivial trajectories of the computational initial states on the Bloch sphere. (a) Trajectory of* $|01\rangle$*. (b) Trajectory of* $|11\rangle$*. Figures from Ref. [10]*

2.2.3 Three-Qubit Gates

Along with the two-qubit gates, research on quantum three-qubit gates has considerably increased in the last years, as peculiar characteristics offered by these gates enhance the quality of quantum computing processing. The idea of a 3-bit gate, which performs operations on three bits simultaneously, was first introduced by Tommaso Toffoli in 1980, with the classical Toffoli (CCNOT) gate. Being it a reversible logic gate, soon the equivalent quantum gate was introduced. The quantum Toffoli gate consists of a doubly-controlled NOT gate where the state of the target qubit changes depending on the state of the two control qubits. In particular, it performs a NOT operation on the target qubit if and only if both control qubits are in the $|1\rangle$ state, and otherwise leaves the target qubit unchanged [28].

This gate presents several attracting properties: together with a single-qubit gate, it forms a universal set of gates in quantum computation [15]. In addition, it is a key element for faster implementation of some quantum algorithms, such as the Shor's algorithm [29], quantum error correction schemes and fault-tolerant quantum computing [16, 17, 14].

This gate in fact can be decomposed as a sequence of six CNOT gates and several single-qubit gates [30]. Therefore, the significant number of two-qubit and single-qubit gates necessary for its creation increases the number of potential errors that can be made during the computation, thus having a detrimental effect on gate fidelity. Indeed, replacing them with a direct single-shot implementation of the Toffoli gate is of great interest to reduce this error. Furthermore, by using Toffoli gates, not only are we reducing significantly the number of operations, but also the time duration of the computation process. As stated in Subsection 2.1.1, the dominant source of error in the realization of a Rydberg quantum gate is its decoherence time [10]. Therefore, reducing the time spent in the Rydberg state is another crucial advancement we want to make to enhance the gate's fidelity.

The Toffoli gate has been successfully demonstrated with atomic ions [31], but at a relatively low fidelity of 71%, and the duration of the gate was as long as 1.5 ms. The Toffoli gate has also been demonstrated with superconducting qubits at the fidelity of 68.5% [32] and 78% [33]. Whereas in Ref. [14] the gate, realized with ultracold neutral-atom qubits, is shown to be much faster than in the previous cases and can provide approximately 3 μs duration and 96.8% fidelity.

Overall, we have now convinced ourselves that the Toffoli gate, or generally a quantum three-qubit gate, can be a crucial building block for many quantum algorithms and circuits, speeding up the quantum computing processing and reducing the potential for errors. Bearing this in mind, we now want to investigate the case of a three-qubit gate known as controlled-controlled-phase gate, aiming to realize it with a Rydberg atoms setup and by making use of Quantum Optimal Control Algorithms explained in Chapter 4.

Chapter 3

Check for Complete Controllability

In this chapter, we want to make sure that the controlled-controlled-phase gate can be realized at least from a theoretical point of view, before moving on to its actual realization. In addition, we want to see if we can extract some key information from an initial theoretical analysis that can facilitate the optimization of the gate. We start by formulating the controlled-controlled-phase gate in braket notation.

$$\mathrm{U_{CCP}} = \sum_{\substack{i,j,k=0 \\ (i,j,k)\neq(1,1,1)}}^{r} |\mathrm{ijk}\rangle\langle\mathrm{ijk}| + e^{i\phi}\,|111\rangle\langle 111| = \mathbb{I} + \left(e^{i\phi} - 1\right)|111\rangle\langle 111| \tag{3.1}$$

In this equation indexes i,j,k assume the values: {0,1,r}. The elements of the sum are three-qubit states, given by the tensor-product of single-qubit states. Each single-qubit state indicates the specific state of one of the 3 Rydberg atoms. There are 3 accessible energy eigenstates, or "levels", for each single-qubit state: the first two, $|0\rangle$ and $|1\rangle$ are encoded into two internal states of the Rydberg atoms, where 0 stands for the ground-level state and 1 for the first excited state. The remaining state $|r\rangle$ is encoded in the Rydberg state of the atom.

We see that given an initial state $|\psi\rangle$, that corresponds to a certain superposition of basis states $\{|000\rangle, ..., |rrr\rangle\}$ the gate acts on it leaving all of its components unvaried except for the $|111\rangle$ component, which is changed by adding a specific phase to it, that most of the time will be set to π, leading to $-|111\rangle$.

We immediately notice that this gate is invariant under permutations of two qubits out of three. To be more clear, this symmetry can be illustrated in the following way: a certain element of the operator is given by $|\mathrm{ijk}\rangle\langle\mathrm{ijk}| = |\mathrm{i}\rangle\langle\mathrm{i}| \otimes |\mathrm{j}\rangle\langle\mathrm{j}| \otimes |\mathrm{k}\rangle\langle\mathrm{k}|$, that is the tensor product of three components, the first of which acts on the first qubit state, the second on the second and the third on the third. At this point, if we exchange the states of two of the qubits, such as the first and the second states, we obtain $|\mathrm{jik}\rangle\langle\mathrm{jik}|$, and if we repeat the permutation for all of the gate's elements we end up obtaining the exact same gate defined in Eq. (3.1).

This peculiar property of the gate highlights an important aspect to take into account for its realization: the gate is given by a certain combination of operators that are invariant under the permutation of two qubits out of three. At this point we want to analyze this aspect more rigorously by introducing the following permutation operators:

$$\begin{aligned} \mathrm{P_{12}} &= \sum_{i,j,k=0}^{r} |\mathrm{ijk}\rangle\langle\mathrm{jik}| \text{ operator that exchanges the states of the first two qubits} \\ \mathrm{P_{23}} &= \sum_{i,j,k=0}^{r} |\mathrm{ijk}\rangle\langle\mathrm{ikj}| \text{ operator that exchanges the states of the last two qubits} \end{aligned} \tag{3.2}$$

We notice that there is no need to introduce the third permutation operator that exchanges the first and the third state, as a combination of these two operators is sufficient to obtain any other permutation, including the one between the first and third state. We now understand that an operator

is permutation-invariant[1] only if it commutes with both permutation operators and this mathematically translates into:

$$\mathcal{O} \text{ is permutation-invariant} \iff \begin{cases} [\mathcal{O}, \mathrm{P}_{12}] = \mathcal{O}\mathrm{P}_{12} - \mathrm{P}_{12}\mathcal{O} = 0 \\ [\mathcal{O}, \mathrm{P}_{23}] = \mathcal{O}\mathrm{P}_{23} - \mathrm{P}_{23}\mathcal{O} = 0 \end{cases} \tag{3.3}$$

3.1 System Setup

Now, having noticed this peculiar symmetry, we figure out that the best geometrical arrangement for the three Rydberg atoms is an equilateral triangle, that indeed presents the same symmetry as the gate. Furthermore, in view of many-body quantum computation where many atoms are packed together in an optical lattice, the triangular geometric layout here suggested would indeed maximize the number of atoms that can be placed in a certain area. In fact, given a circle of radius r, if we aim to place as many circles as possible on a plane, the best layout to adopt is to place the circle centers in equilateral triangular arrangements.

Therefore, this disposition leads to higher connectivity between Rydberg atoms, that implies stronger interactions, thus improving the quality of the Rydberg blockade effect on nearby atoms. Overall, this results in an improvement of the gate's fidelity as well as more efficient quantum parallelism.

To formulate the Hamiltonian of the three-qubit system, we recall that the gate is achieved by coupling the $|0\rangle$ and $|1\rangle$ states to a strongly interacting Rydberg state $|r\rangle$ by driving precise laser pulses on the Rydberg atoms [2]. In this case, we simplify the system by driving one homogeneous laser beam on all atoms, in analogy with Ref. [10]. Therefore, we assume the Hamiltonian governing the dynamics of the system to be of the form:

$$\mathrm{H} = \mathrm{H}_0 + \mathrm{H}_{int} \tag{3.4}$$

The first term, H_0 accounts for the coupling to the Rydberg state by means of the laser electromagnetic field and can be controlled by manipulating the lasers' parameters. The second term H_{int} accounts for the strong dipole-dipole interaction taking place between adjacent atoms when they are in the Rydberg state (see Subsection 2.1.2). In particular, H_0 describes the coupling to the Rydberg state within the rotating frame and applying the rotating wave approximation[2]:

$$\mathrm{H}_0 = \sum_{j=1}^{3} \left[\Omega^{01}(t) \left(|0\rangle\langle 1| + |1\rangle\langle 0| \right)_j + \Delta^{01}(t) \left(|1\rangle\langle 1| \right)_j + \Omega^{1r}(t) \left(|1\rangle\langle r| + |r\rangle\langle 1| \right)_j + \Delta^{1r}(t) (|r\rangle\langle r|)_j \right] \tag{3.5}$$

In this equation, we imply that the one-qubit components indexed with j (where j indicates the number of the qubit considered) are equivalent to three-qubit components given by the tensor product of two identity operators acting on the other two qubits and the one-qubit component taken into account. For example,

$$\left(|0\rangle\langle 1| + |1\rangle\langle 0| \right)_1 \equiv \left(|0\rangle\langle 1| + |1\rangle\langle 0| \right)_1 \otimes \mathbb{I}_2 \otimes \mathbb{I}_3 \tag{3.6}$$

where $\mathbb{I}_2 = |0\rangle\langle 0|_2 + |1\rangle\langle 1|_2 + |r\rangle\langle r|_2$ represents the identity operator that acts on the second qubit's state, and the same goes for $\mathbb{I}_3$.

Furthermore, in Equation (3.5), Ω and Δ are the parameters that characterize the dynamics of the system and the coupling of the atomic states. In particular, Ω^{01} and Ω^{1r} represent the time-dependent Rabi frequencies at which the coupling between states $|0\rangle$ $|1\rangle$ and between states $|1\rangle$ $|r\rangle$ occurs. Whereas Δ^{01} and Δ^{1r} represent the time-dependent detuning parameters (see Section 2.2).

The interaction between the Rydberg states reduces to

$$\mathrm{H}_{int} = \frac{C_6}{R^6} \sum_{\substack{i,j=1 \\ i \neq j}}^{3} |rr\rangle_{ij} \langle rr|_{ij} \tag{3.7}$$

[1] from this point onwards by saying permutation-invariant we will always refer to invariance under permutations of two qubits out of three

[2] This equation is the generalization of Eq. (2.13), which describes the Hamiltonian of controlled-phase gate

By recalling Subsection 2.1.2, this term describes the dipole-dipole (van der Waals) interaction between adjacent Rydberg states $|r\rangle_i$ and $|r\rangle_j$, where C_6 describes the instantaneous dipole-dipole interaction and R defines the inter-atomic distance, that is the separation between the centers. $V = C_6/R^6$ denotes the interaction strength. We note that having placed the atoms in an equilateral triangle the inter-atomic distance R is the same for all pairs of atoms.

3.2 Check 1: matching between space of permutation commutants and Lie Algebra

Having defined the Hamiltonian of the system in Eq. (3.5) and having highlighted the invariance property of the c-c-phase gate, we now want to test whether the Hamiltonian has complete controllability over the gate. In other words, we want to check the feasibility of the gate given this particular Hamiltonian, and to achieve this, we carry out a series of tests written in the Scientific Programming Language GNU Octave[3].

Firstly, we want to verify whether the Lie Algebra given by the Hamiltonian matches the vector space of the operators that are invariant under permutations of two qubits out of three. This would ensure that the gate can be obtained from the Lie Algebra since we already mentioned that the gate must be a combination of permutation-invariant operators. To simplify the verification, we notice that the Hamiltonian is also permutation-invariant, a predictable result since it describes a geometrically symmetrical system. Hence, to verify whether the two spaces match we can settle for a mere comparison between the dimensions of the two vector spaces.

We now proceed to compute the Lie algebra generated by the Hamiltonian. To do so, we define the Lie Algebra generators in the following way:

$$\begin{aligned}
A &= (|0\rangle\langle 1| + |1\rangle\langle 0|)_1 \otimes \mathbb{I}_2 \otimes \mathbb{I}_3 + \mathbb{I}_1 \otimes (|0\rangle\langle 1| + |1\rangle\langle 0|)_2 \otimes \mathbb{I}_3 + \mathbb{I}_1 \otimes \mathbb{I}_2 \otimes (|0\rangle\langle 1| + |1\rangle\langle 0|)_3 \\
B &= (|1\rangle\langle 1|)_1 \otimes \mathbb{I}_2 \otimes \mathbb{I}_3 + \mathbb{I}_1 \otimes (|1\rangle\langle 1|)_2 \otimes \mathbb{I}_3 + \mathbb{I}_1 \otimes \mathbb{I}_2 \otimes (|1\rangle\langle 1|)_3 \\
C &= (|1\rangle\langle r| + |r\rangle\langle 1|)_1 \otimes \mathbb{I}_2 \otimes \mathbb{I}_3 + \mathbb{I}_1 \otimes (|1\rangle\langle r| + |r\rangle\langle 1|)_2 \otimes \mathbb{I}_3 + \mathbb{I}_1 \otimes \mathbb{I}_2 \otimes (|1\rangle\langle r| + |r\rangle\langle 1|)_3 \\
D &= (|r\rangle\langle r|)_1 \otimes \mathbb{I}_2 \otimes \mathbb{I}_3 + \mathbb{I}_1 \otimes (|r\rangle\langle r|)_2 \otimes \mathbb{I}_3 + \mathbb{I}_1 \otimes \mathbb{I}_2 \otimes (|r\rangle\langle r|)_3 \\
V &= (|rr\rangle\langle rr|)_{12} \otimes \mathbb{I}_3 + (|r\rangle\langle r|)_1 \otimes \mathbb{I}_2 \otimes (|r\rangle\langle r|)_3 + \mathbb{I}_1 \otimes (|rr\rangle\langle rr|)_{23}
\end{aligned} \tag{3.8}$$

These operators are called the generators of the Hamiltonian due to the fact that if we combine them with the respective Ω and Δ parameters and sum them together we obtain the Hamiltonian defined in Eq. (3.5). Consequently, we ideate an algorithm to create the Lie Algebra. The idea behind the algorithm consists of the following steps: We write the operators in Eq. (3.8) as matrices, and then proceed to write each operator as a single-dimensional array by stacking its columns one on top of the other, starting with the first on top, the second beneath it, and so on. We then form a matrix named CO (control matrix) with each operator as a column of the matrix (for example column 1 = operator A written as column). CO represents the matrix whose columns are the elements of the Lie Algebra. We then normalize each column making them unitary vectors. We then orthogonalize the columns by applying the "orth" function in Octave, thus obtaining an orthonormal basis B_{CO}.

We then proceed to generate a new element X of the algebraic Lie closure. X is obtained by computing the commutator $i[\mathcal{O}_1, \mathcal{O}_2] = \mathrm{X}$[4] where $\mathcal{O}_1$ and $\mathcal{O}_2$ are two operators taken from the elements in the Lie Algebra. If X is linearly dependent to the other elements in the algebra, we discard it, otherwise we add it to the matrix as its last column, hence adding it to the set of generators and elements contained in the Lie Algebra. To check if X is linearly dependent to the elements of the Algebra we:

1. initially check if its norm is greater than a minimum benchmark (mb), set to 10^-12. If the norm is less than mb we discard it, since we assume the norm to be equal to 0. This passage must be done in our procedure to avoid the traps of roundoff errors, introduced by the computer due to

[3]GNU Octave, version 4.4.1 Copyright (C) https://octave.org

[4]we multiply the commutators for the immaginary unit "i" because with this operation, if $\mathcal{O}_1$ and $\mathcal{O}_2$ are Hermitian, also X is Hermitian. In this way, we are generating an Algebra of Hermitian Operators over the real Field

the finite number of digits used to compute the operations, meaning that a zero could be written as $10^{-}16$. Since the columns consist of 729 complex components, if for a column we assume each component to be $v_i = 10^{-}16 + i10^{-}16 = 0$, the norm of the resultant vector is around $10^{-}12$, thus considered equal to 0. If the norm is greater than mb we go to the next step.

2. make use of the Gram-Schmidt method. The method consists of discarding the components of the X vector projected on the basis vectors $\in B_{CO}$ as this would lead to obtain a vector X' that is orthogonal to B_{CO}. Let us use the braket notation by calling $X = |v\rangle$ and the orthonormal vectors $\{|w_1\rangle, |w_2\rangle, .., |w_n\rangle\}$. The orthogonalization of $|v\rangle$ is achieved by applying the following formula:
$$|v\rangle = |v\rangle - \sum_{i=1}^{N} \langle w_i|v\rangle |w_i\rangle \tag{3.9}$$

3. We now check if $\sqrt{\langle v|v\rangle} \geq bm$. If it is greater, we normalize it to 1 and then add it to the CO matrix, otherwise we discard it.

We repeat the previous step for all possible pairs of elements contained in the Algebra, therefore for all possible combinations of pairs of columns in the CO matrix, obtaining, in the end, a matrix given by a set of orthonormal columns that correspond to all of the elements contained in the algebraic Lie closure of the Hamiltonian. Now, given this set of columns, every operator obtained by computing the commutator of two columns of CO, Y $= i$[column 1, column 2] can be always obtained by a specific linear combination of the columns of the matrix, or in other words, the operator is contained in the Lie Algebra.[5] By running this algorithm, we find the dimension of the Algebra to be equal to 164.

Note that this algorithm was first realized by checking the linear dependence of the columns by checking the rank of the CO matrix, making use of the "rank" function in Octave, instead of the Gram-Schmidt method. This method was then replaced to cope with the roundoff errors that would lead to anomalies in the third testing phase described in Section 3.4.

Note also that the norm of the vectors used in the algorithm is the Euclidean norm, which is defined as the square root of the inner product of a vector with itself. But we remember that the vectors were actually operators written in columns, therefore we recognize that the Euclidean norm applied to vectors corresponds to the matrix norm induced by the Hilbert-Schmidt trace $Tr(A^{\dagger}B)$, called Frobenius norm [34]. This norm is rigorously defined in Subsection 4.3.1.

Let us now derive the dimension of the space given by permutation-invariant operators. Recalling Eq. (3.3), we remember that if an operator is permutation-invariant, it commutes with the permutation operators P_{12}, P_{23}, hence the name "permutation commutants". Bearing this in mind, we can reformulate the commutators in a more convenient way by first defining the following operators:

$$\begin{aligned} \mathcal{M}_{12} &= -P_{12} \otimes \mathbb{I} + \mathbb{I} \otimes P_{12}^{\dagger} \\ \mathcal{M}_{23} &= -P_{23} \otimes \mathbb{I} + \mathbb{I} \otimes P_{23}^{\dagger} \end{aligned} \tag{3.10}$$

At this point, we can quite straightforwardly see that $[\mathcal{O}, \mathrm{P}_{12}] = \mathcal{M}_{12}(\mathcal{O}) = 0$, $[\mathcal{O}, \mathrm{P}_{23}] = \mathcal{M}_{12}(\mathcal{O}) = 0$, where the second terms of the equations denote the application of the operator $\mathcal{O}$ written as a vector (columns stacked one on top of the other) to the $\mathcal{M}$ operators.

This reformulation offers us the key to finding the invariant-permutation operators' space dimension. Indeed, we can think of this space as the kernel of the $\mathcal{M}$ matrix given by stacking $\mathcal{M}_{12}$ $\mathcal{M}_{23}$ one on top of the other. Making use of simple functions offered by Octave, we find the dimension to be equal to 164.

We observe that the two spaces are not equivalent, and as we expect, the one out of the two which has a higher dimension is the space of permutation-invariant operators, which therefore contains the Lie Algebra. This result introduces the slight chance for us not to be able to realize the c-c-phase gate since the element missing from the Lie Algebra could be crucial for the construction of the gate.

[5] This property corresponds to the definition of Closed Lie Algebra.

3.3 Check 2: c-c-phase gate generated by the Lie Algebra

Secondly, we now proceed with a more straightforward verification. We want to directly check if the c-c-phase gate can be generated by the elements in the Lie Algebra derived in Section 3.2. This translates into checking if the generator of the gate, that we will refer to as target Hamiltonian H_T, can be obtained as a linear combination of elements in the Lie Algebra. The condition for which the Algebra Lie element H_T generates the c-c-phase gate is given by [35]:

$$U_{CCP} = \exp(i\phi H_T) = \mathbb{I} + i\phi H_T - \frac{\phi^2}{2} H_T^2 + \dots \tag{3.11}$$

Therefore, we understand that the generator of the gate is given by $H_T = |111\rangle\langle 111|$. In fact

$$\exp(i\phi H_T) = \mathbb{I} + i\phi\,|111\rangle\langle 111| - \frac{\phi^2}{2} 111111 + \dots = \mathbb{I} + (e^{i\phi} - 1)\,|111\rangle\langle 111| = U_{CCP} \tag{3.12}$$

In matrix notation, we have:

$$H_T = \begin{pmatrix} 0 & 0 & \dots & 0 & 0 \\ \vdots & \ddots & \dots & 0 & \vdots \\ 0 & \dots & 1 & \dots & 0 \\ \vdots & 0 & \dots & \ddots & \vdots \\ 0 & 0 & \dots & 0 & 0 \end{pmatrix} \xrightarrow{e^{i\phi H_T}} U_{CPP} = \begin{pmatrix} 1 & 0 & \dots & 0 & 0 \\ \vdots & \ddots & \dots & 0 & \vdots \\ 0 & \dots & e^{i\phi} & \dots & 0 \\ \vdots & 0 & \dots & \ddots & \vdots \\ 0 & 0 & \dots & 0 & 1 \end{pmatrix} \tag{3.13}$$

Let us now proceed with the testing. We write H_T as a column, and add it to the CO matrix, which we know represents the Lie Algebra of the Hamiltonian. We then orthogonalize H_T with respect to the orthonormal columns of CO by using the Gram-Schmidt method illustrated in Section 3.2. We find the norm to be equal to 0.086, meaning that the generator is not obtainable as a linear combination of the only operators in the Lie Algebra: $H_T \notin CO$. Hence, the c-c-phase does not seem to be obtainable starting from the Hamiltonian described, which then implies our inability to create the c-c-phase gate with this particular system of 3 Rydberg atoms.

However, we can find an alternative solution. Indeed, what we are trying to obtain is a gate that has complete control over all the possible three-qubit states, including the Rydberg states. Instead, we discover that this request can be slightly weakened since there is no need to have complete controllability over the Rydberg state for the quantum computation algorithms we are aiming to implement.

The crucial aspect to focus on is that Rydberg state is merely a support state that permits us to realize the gate by coupling the $|0\rangle$ $|1\rangle$ states with $|r\rangle$, but once the gate's duration is ended, the Rydberg state is no longer considered (see Subsection 2.1.2). Therefore, we can choose to limit the gate's control over the 8 computational three-qubit states, where no Rydberg states are present. Let us call this the logical basis: $\mathbb{B} = \{\ |000\rangle, |001\rangle, |010\rangle, |011\rangle, |100\rangle, |101\rangle, |110\rangle, |111\rangle\ \}$. The gate must leave all of the computational states unvaried except for the $|111\rangle$ state which is manipulated by the gate with an addition of a certain phase to it, $e^{i\phi}\,|111\rangle$. In this way, we do not have complete controllability over the system, but we do have controllability over the actual states that we want to manipulate.

The restriction to the $\mathbb{B}$ basis mathematically corresponds to applying a change of basis operator $\mathcal{C}$ to the c-c-phase operator. Let us define the operator $\mathcal{C}$:

$$\mathcal{C} = |1\rangle\langle 000| + |2\rangle\langle 001| + |4\rangle\langle 010| + |5\rangle\langle 011| + |10\rangle\langle 100| + |11\rangle\langle 101| + |13\rangle\langle 110| + |14\rangle\langle 111| \tag{3.14}$$

In this equation the ket states are written in the "full" basis of 27 three-qubit states which include the Rydberg state (ranging from $|000\rangle$ to $|rrr\rangle$), and the number of each state indicates its position in the basis[6]. Let us call this the $\mathcal{B}$ basis. The bra states instead are written in full extent in the 8 states computational basis $\mathbb{B}$ (discarding the Rydberg states). So what we are doing is transforming a vector

[6]For example, the state $|11\rangle_{position} = |101\rangle_{basis}$ is the 11^{th} state of the complete computational basis.

written in the $\mathbb{B}$ basis to the same vector written in the complete basis $\mathcal{B}$. Therefore, to restrict the gate's action to $\mathbb{B}$ we apply $\mathcal{C}$ in the following way: $\tilde{U}_C = U_{CCP} \cdot \mathcal{C}$

Another way to figure this is by writing the gate in matrix notation in the full-basis (27×27) and rearranging it by placing the 8 columns that match the ones of $\tilde{U}_C$ at the left of the matrix. Thus obtain:

$$U_{CPP} = \left(\begin{array}{c|c} \tilde{U}_C & \mathbf{0} \\ & \mathrm{R} \end{array}\right) = \left(\begin{array}{c|c} \tilde{U} & \mathbf{0} \\ \hline \mathbf{0} & \mathrm{R} \end{array}\right) \tag{3.15}$$

where we apply no restrictions to the matrix block R, whereas $\tilde{U}$ must operate as a controlled-controlled-phase gate on the two computation levels $|0\rangle$ and $|1\rangle$, namely on the $\mathbb{B}$ basis: $\tilde{U} = \mathbb{I} + (e^{i\phi} - 1)\,|111\rangle\langle 111|$. In simple words, by applying $\mathcal{C}$ we are filtering the gate and only focusing on 8 columns out of 27.

The question we now have to answer is: how can we check if the gate in Eq. (3.15) is generated by the Lie Algebra of the Hamiltonian? We simply verify whether the first 8 columns of its generator, $\tilde{H}_T$, are given by a linear combination of the Lie Algebra restricted to the logical basis obtained by applying the change of basis operator $\mathcal{C}$ to all of its elements. This is because we have generated the Lie Algebra so that all of its elements are Hermitian operators (by adding the immaginary unit in the commutator, see Section 3.2). Therefore, if the first 8 columns of the generator are given by:

$$\tilde{H}_T = \left(\begin{array}{c} \tilde{H} \\ \hline \mathbf{0} \end{array}\right) \tag{3.16}$$

With $\tilde{H} = |111\rangle\langle 111|$ written in the logical basis, since the operator is hermitian, the generator in the full basis must be of the form: $H_T = \left(\begin{array}{c|c} \tilde{H} & \mathbf{0} \\ \hline \mathbf{0} & \mathrm{M} \end{array}\right)$ Finally, we can convince ourselves that by calculating $\exp(i\phi \mathrm{H}_T)$ with H_T defined as a block matrix, we obtain U_{CPP} defined in Eq. (3.15).

Now, by writing $\tilde{H}_T$ and the elements of the restricted Lie Algebra $\tilde{CO}$ as vectors (see Section 3.2), we now apply the Gram-Schmidt method to $|\tilde{H}_T\rangle$. Therefore we calculate the inner product of $|\tilde{H}_T\rangle$ with each component of the Lie Algebra, and subtract it to $|\tilde{H}_T\rangle$, obtaining a new vector $|\tilde{H}'_T\rangle$ that is orthogonal to the Lie Algebra basis $B_{\tilde{CO}}$. Thus, we find its norm to be $\| |\tilde{H}'_T\rangle \| = 1.5 \cdot 10^{-15} < mb = 10^{-12}$. This implies that the c-c-phase gate generator $\tilde{H}_T$ is given by a linear combination of the Lie Algebra restricted to the logical basis.

Therefore, with no spared efforts, we are now convinced that we can build a c-c-phase gate that has complete controllability over the 8 computational states of the $\mathbb{B}$ basis.

3.4 Check 3: negligible time-dependent parameters

Since the check for complete controllability was no easy work to conclude, we do not expect the realization of the gate to be intuitive. Indeed, we cannot find easy theoretical thought-out ways to construct the gate. That is why we directly aim to build the gate by making use of Optimal Control Algorithms, where the time-dependent parameters are manipulated in a certain way to achieve the gate. In sight of this, we want to carry out one last check, that aims to facilitate the realization of the gate by verifying whether some of the time-dependent parameters can be excluded, therefore restricting the number of time-dependent parameters that are to be handled.

The process remains the same as the one laid out in Section 3.2, with the only difference being that in this case the Lie Algebra is not generated by all of the operators defined in Eq. (3.8). We exclude one generator at a time and generate the Lie Algebra with the remaining ones and then proceed to check whether the c-c-phase gate restricted to the $\mathbb{B}$ basis can be obtained by the Lie Algebra or not. For instance, by excluding the A operator, we then generate the Lie Algebra with B, C, D and V, and finally, we check if the c-c-phase gate is a linear combination of this Lie Algebra.

Excluded Gen.	**Excluded Par.**	**Lie Dimension**	$\|\mathrm{H}_T\|_F$	$\|\tilde{\mathrm{H}}_T\|_F$	**c-c-phase**
A	Ω_{01}	31	0.22	$6 \cdot 10^{-16}$	no
B	Δ_{01} and Δ_{1r}	164	0.09	$6 \cdot 10^{-16}$	yes
C	Ω_{1r}	6	0.84	0.71	no
D	Δ_{1r}	164	0.09	$2 \cdot 10^{-15}$	yes
V	C_6/R^6	9	0.86	0.71	no
B and D	Δ_{01} and Δ_{1r}	163	0.17	10^{-15}	yes
A, B and D	Δ_{01}, Δ_{1r} and Ω_{01}	28	0.29	$9 \cdot 10^{-16}$	yes

Table 3.1: *Results on whether generators and respective parameters can be excluded or not for the realization of the c-c-phase gate.* $\|\mathrm{H}_T\|_F$ *denotes the Frobenius norm of the generator of the c-c-phase gate written in the full basis (*27×27*).* $\|\tilde{\mathrm{H}}_T\|_F$ *denotes the Frobenius norm of the generator restricted to the logical basis (*27×8*)*

We notice that generators A, B and D can be neglected in the realization of the gate, and this gives us a precious hint on how to manipulate their respective time-dependent parameters, Δ^{01}, Δ^{1r} and Ω_{01}. We indeed expect that we can fix these parameters to constant values, and limit ourselves to vary the Rabi frequency Ω^{1r} in time.

In addition, the testing carried out without considering the interaction term in generating the Lie Algebra confirms what previously stated in Subsection 2.1.2. Without the dipole-dipole interaction between atoms, which leads to the Rydberg blockade effect, it is impossible to create the gate. In fact, the controlled-controlled-phase gate requires entangling properties of the physical system in order to be realized.

Chapter 4

Optimization of the Gate

What we are now trying to accomplish is the optimization of the controlled-controlled-phase gate. To better understand what we are talking about let us briefly outline what the Quantum Optimal Control Theory (QOCT) is about. As we have mentioned in Chapter 2 and 3, the gate is obtained by applying a global laser on the Rydberg atoms, which triggers the coupling of the intrinsic atomic states that depend on certain time-dependent Rabi frequencies $\Omega(t)$ and detuning parameters $\Delta(t)$. After the duration τ of the laser, the outcome of the dynamics is that a certain initial state of the Rydberg system has been transferred to a final one.

Our aim is to tailor the laser pulses in order to control the dynamics of the system, that in our case means to find the optimal pulse which leads to the realization of the c-c-phase gate, and here is where QOCT intervenes. The basic concept behind this theory is that the definition of an optimal pulse follows from the variation of a properly defined functional [36].

Another aspect we should also consider is that the decay time of the Rydberg state is the biggest source of error that deteriorates the gate fidelity, as stated in Subsection 2.1.1. Therefore the optimization should focus both on shaping the pulse and reducing the time duration of the gate, finding the sweet spot in time where there is little decoherence but sufficient time to couple the states. In this analysis, we neglect the error introduced by the decoherence, and focus on optimizing the pulses.

4.1 Quantum Optimal Control Problem

To analyze the theory more in depth, let us consider a generic QOC problem, generally defined as control problem, which can be outlined through the dynamics of a quantum system[1], and an optimization target [18]. The system starts in an initial state $|\Psi_0\rangle$ and evolves according to the time-dependent Schrödinger's equation:

$$\frac{\partial}{\partial t}|\Psi(t)\rangle = -\frac{i}{\hbar}\mathrm{H}|\Psi(t)\rangle \tag{4.1}$$

In the case of a closed[2] quantum system, the solution to Equation (4.1) is given by

$$|\Psi(t)\rangle = \mathrm{U(t)}\,|\Psi_0\rangle \tag{4.2}$$

With the unitary propagator

$$\mathrm{U(t)} = \mathcal{T}\exp\left(\int_0^t \mathrm{H(t)}d\tau\right) \tag{4.3}$$

where $\mathcal{T}$ is the Dyson time-ordering operator [37].

Consequently, the functional we want to minimize has to quantify the distance between the final state, resulting from the time evolution of the initial state, and the optimization target, which is the state we would obtain from the time evolution following the dynamics we are aiming to achieve [18].

[1] The dynamics in our case consists of the interaction between the laser and the Rydberg atoms

[2] By saying that the system is closed we intend that there is no interaction between the system and the external environment and we take this assumption to be valid also for our problem

The functional is called Figure of Merit (FoM). Such FoM can be the state overlap fidelity, or also the gate overlap fidelity. They are defined as:

$$F_{state} = \| \langle \Psi_T | \Psi_{aim} \rangle \|^2 \quad F_{gate} = \frac{1}{N^2} \mathrm{tr} \left(U_{aim}^{\dagger} U_T \right) \tag{4.4}$$

The only thing left to do is to link the optimization of the laser to the minimization of the functional, which would imply the resolution of the control problem. To face these kind of control problems, the CRAB (Chopped Random Basis) algorithm and its recursive version dCRAB (dressed CRAB), have proven to be effective and efficient [38]. To fully describe their procedure let us now introduce a specific Python library named QuOCS (Quantum Optimal Control Suite) [18] where these algorithms are defined.

4.2 CRAB and dCRAB Algorithms

Firstly, let us transfer the control problem from the optimization of the laser pulse to the one of its 4 time-dependent parameters, detunings Δ_{01}, Δ_{1r}, and Rabi frequencies Ω_{01} and Ω_{1r}, that we can name control fields or control pulses f(t) [18]. Let us now describe the main features of the algorithm and its main steps applied to this specific case.

The main idea of the dCRAB algorithm is to make a randomized truncated expansion of the pulse in a given basis, for example in Fourier series [38, 10]. The Fourier series is defined as:

$$g(t) = 1 + \frac{\left[\sum_{n=1}^{N_c} \mathrm{A}_n \sin(\omega_n t) + \mathrm{B}_n \cos(\omega_n t) \right]}{\lambda(t)} \tag{4.5}$$

with coefficients $\{A_i, B_i, \omega_i\}$, where i is the base index.

The main steps of the algorithm in our specific case are:

1. Assign the initial values to the parameter pulses.

2. Simulate the dynamics by calculating the time evolution of a smartly chosen initial state (which will be rigorously defined in Subsec. 4.3.1). To compute the time evolution, we use Eq. (4.2), where the unitary operator U_i defined in Eq. (4.3) is calculated considering the Hamiltonian defined in Eq. (3.5). Here the Hamiltonian time-dependent parameters take the values initially assigned.

3. Calculate the FoM as the state or gate overlap fidelity, defined in Eq. (4.4) where the target unitary operator U_T corresponds to U_{CPP}, the c-c-phase gate, and $U_{aim} = U_i$, that is the unitary operator that we just calculated with this initial set of parameter pulses. In general, the procedure of step 2 and 3 can be condensed into a single function named "get_FoM", which takes the parameter pulses as an input, and returns the FoM as an output [18]. We can define this function as $\mathcal{F} := \mathcal{F}(f(t))$. Furthermore, being the parameter pulses expanded in basis functions with coefficients $\{A, B_i, \omega_i\}$, this implies that $\mathcal{F}(f(t)) = \mathcal{F}(A_1, B_1, \omega_1, ..., A_n, B_n, omega_n)$.

4. Update the set of coefficients $\{A_i, B_i, \omega_i\}$ in order to minimize $\mathcal{F}$ with direct-search methods, which can be either gradient-free such as Nelder-Mead simplex method algorithm, or gradient-based as the CMA-ES [38]. Return then to step 2.

By setting stopping criteria in the minimization algorithm we conclude our optimization. In a nutshell, by using this algorithm the control problem given by the minimization of a functional (FoM), is recast to a multivariable function minimization that can be performed via direct-search methods [38].

Note that defining the "get_FoM" function as in step 3 would lead us to a maximization problem. If we want to solve a minimization problem, which is the actually solvable one, the FoM must be redefined as an object called "infidelity", that goes to zero as the gate's fidelity reaches its maximum value. An example of infidelity would be:

$$\text{infidelity} = 1 - FoM \tag{4.6}$$

where we have normalized the FoM so that its maximum value (perfect overlap between the two gates) is equal to 1.

Now, let us consider the pulse $f(t) \in L_2$, where L_2 is the function space of square-integrable functions. By using a limited number N of basis functions to describe $f(t)$, we risk to get trapped in a local minimum that we might mistake for the global one, since we are performing the optimization in a restricted space of dimension N. This is known as a false trap. To cope with this, the CRAB algorithm chooses randomly the basis functions e.g. in a Fourier basis the frequencies ω_i are chosen stochastically in a fixed interval. To further avoid false traps, we can use the improved version of the CRAB algorithm called dCRAB. Its key feature is to reiterate the CRAB algorithm each time with an initial pulse equal to the final one of the previous iteration. Those iterations are called super-iterations, so as to distinguish them from the ones of the coefficients' optimization. Once we start a new super-iteration "I2", we have already optimized the coefficients of the N basis functions considered in the previous one "I1", so the algorithm proceeds to expand the parameter pulses into newly randomly chosen basis functions summed to the ones previously optimized. At this point, it optimizes the pulses by optimizing the coefficients of the new basis functions. To simplify the notation let us compactly denote the coefficients as $\{A_i, B_i, \omega_i\} = c_i$. Thus, the j-th super-iteration restricts the optimization only to $c_i^j, i = 0, 1..N$ of

$$f^j(t) = c_0^j f^{j-1}(t) + \sum_{i=1}^{N} c_i^j f_i^j(t) \ , \tag{4.7}$$

where f^{j-1} is the pulse obtained from the previous super-iteration and f^j are the new basis functions randomly chosen.

Let us highlight that by using the dCRAB algorithm, supposing we get stuck in a false trap, the probability of adding a new random direction and remaining in the false trap is zero because of the infinite possible choices of basis [39].

To conclude, the truncation of basis in the CRAB or dCRAB algorithm translates to a natural arise of bandwidth limits which contribute to the capability of these algorithms to encompass experimental constraints [40]. In fact, high bandwidth of the pulses is extremely challenging to achieve in the experimental setup [10].

4.3 Optimization with QuOCS

Finally, we can now proceed with the actual realization of the c-c-phase gate. We start by displaying the hints offered by the analysis carried out in Chapter 3, taking them as starting points for an efficient optimization procedure.

1. We must restrict the gate's control over the actual computational states ($\mathbb{B}$ basis)

2. We can presumably limit ourselves to vary the Rabi frequency Ω^{1r} in time while fixing the other parameters to constant values.

From Section 4.1 we know that optimizing the laser pulse corresponds to optimizing the system's parameters Δ and Ω (control fields). To accomplish this, we make use of the QuOCS library in Python[3].

4.3.1 Creation of the "get_FoM" function

The core of the algorithm is the creation of the get_FoM function that resembles our optimization problem. Let us call this function $\mathcal{F}$. We remember that we need to "feed" $\mathcal{F}$ with the parameter pulses for it to return the FoM, which is the value we want to minimize. Practically, since we use numerical computational methods to solve the problem, we must discretize the time duration of the dynamics in a finite number of time steps, and that implies a discretization of the parameter pulses. Hence, we create a list that defines the timegrid and for each parameter a list where the i-th element

[3]Python 3.11.2 https://www.python.org

of the list defines the value assumed by the parameter at the i-th timestep. These lists are then passed as an argument to $\mathcal{F}$.

Let us now use the second hint defined at the beginning of the section, which implies that there is no need to optimize all 4 parameter pulses. In fact, the only one that plays a significant role in the realization of the gate and that consequently controls the dynamics of the system is the Rabi frequency Ω^{1r}. This reduces to excluding the detuning parameters and the Rabi frequency Ω_{01} from the optimization, fixing them to constant values initially set to 1, therefore all we have to do is define them only once in the Get_FoM function's environment, whereas the list of the Rabi frequency has to be updated by the algorithm and called by $\mathcal{F}$ in every iteration.

The next step is to calculate the time evolution of a generic initial state, within the $\mathcal{F}$ function. We have a list of time-steps at our disposal, and we can use numerical computing algorithms to calculate the integral in Eq. (4.3) such as the ones defined in the QuTiP library. However, differently from the general method explained in Section 4.1, we decide to calculate the time evolution by applying a first order approximation on the Hamiltonian. We assume the Hamiltonian to be sufficiently constant in the time interval equal to the time-step considered. Therefore, we can locally assume for the time-evolution to be well described by the time-dependent Schrödinger equation:

$$|\Psi(t_2)\rangle = e^{-i\frac{\mathrm{H}(\mathrm{t}_1)}{\hbar}dt}\,|\Psi(t_1)\rangle \Longleftrightarrow U(t_2) = e^{-i\frac{\mathrm{H}(\mathrm{t}_1)}{\hbar}dt}U(t_1) \tag{4.8}$$

Where the Hamiltonian is constant, giving us the vector state's evolution from t_1 to t_2, where t_1 and t_2 represent two adjacent values of time in the time grid list, with time-step $dt = t_2 - t_1$. Thus, we can calculate the time-evolution operator for the whole duration of the gate by iteratively calculating the local time evolution for each time-step:

$$U_{aim}(t) = \prod_{i=1}^{N} e^{-i\frac{\mathrm{H}(\mathrm{t_i})}{\hbar}dt} \tag{4.9}$$

Where N is the number of time steps defined in the time grid list and the Hamiltonian is the one defined in Eq. (3.5). Let us stress that the Hamiltonian, which depends on the time-dependent parameters, is calculated at time t_i (i-th element of the time grid list) by setting each parameter, in our case $\Omega^{1r}(t_i)$, equal to the i-th element of the respective parameter pulse's list. The detunings, Δ^{01} and Δ^{1r} and Rabi frequency Ω^{01} are instead fixed to constant values. The Van der Waals coefficient $\frac{C_6}{R^6}$ is set to the constant value know from Subsection much greater than the one of the parameters considered. In fact, recalling 2.1.2, we need to impose this condition if we want the system to be close to the ideal regime of Rydberg blockade ($V \gg \hbar\Omega$, $V \gg \hbar\Delta$) and access the entangling features of Rydberg atoms.

At this point, the only thing left to do is the calculation of the Figure of Merit. We now must consider the first hint outlined at the start of the section. Since we only have control over the 8 computational states of the $\mathbb{B}$ basis, we have to restrict the operators to them. Recalling the explanation in Section 3.3, we operate this restriction by applying the change of basis operator $\mathcal{C}$ introduced in Eq. (3.14) to the time-evolution operator U_{aim} and to the c-c-phase gate U_{CCP}:

$$\begin{aligned} \tilde{U}_{CCP} &= U_{CCP} \cdot \mathcal{C} \\ \tilde{U}_{aim} &= U_{aim} \cdot \mathcal{C} \end{aligned} \tag{4.10}$$

Finally, let us now examine the issue of defining the initial state and the optimization target[4]. The first naive approach we could adopt is to choose an initial state given by a superposition of all the computational states of the $\mathbb{B}$ basis, each one contributing to the initial state with the same coefficient $a_i = \frac{1}{2\sqrt{2}}$ with i=1,..,8, in order for the vector state to be normalized. Hence, the optimization target still turns out to be a superposition of all the states, with the coefficients that coincide with the ones of the initial state except for the coefficient of the $|111\rangle$ state, which becomes $a_8 = e^{i\phi}\frac{1}{2\sqrt{2}}$:

$$|\Psi_i n\rangle = \sum_{x=0}^{7} \frac{|\mathrm{x}\rangle}{\sqrt{N}} \xrightarrow{\text{ccp gate}} |\Psi_{fin}\rangle = \sum_{x=0}^{6} \frac{|\mathrm{x}\rangle}{\sqrt{N}} + \frac{e^{i\phi}}{\sqrt{N}}\,|7\rangle \tag{4.11}$$

[4]which is the state resulting from the application of the c-c-phase gate to the initial state, see Section 4.1

With N = 8, number of basis states. The states are written by converting the computational states $|ijk\rangle$ (with i,j,k = 0 or 1) from binary notation to decimal notation: $\left|2^2 i + 2^1 j + 2^0 k\right\rangle$. Now, if we were to calculate the FoM as the state overlap fidelity, we would make a mistake, since the initial state and the optimization target adopted do not fully describe the c-c-phase gate we are considering. That means that we can find many other gates other than the c-c-phase gate which applied to the initial state return the exact same optimization target, therefore the optimization of the parameter pulses could lead to the creation of a generic gate that has nothing to do with the controlled-controlled-phase gate.

An example of a rigorous approach consists of the following passages: calculate the state overlap fidelity for each computational state chosen as initial state, thus obtaining 8 fidelities, then proceed to calculate their norm and sum them. The quantity given by the sum is the one we define as FoM. In fact, in this way we are sure that whatever initial state we choose, which is given by a specific combination of computational states, the final state obtained will coincide with the optimization target.

We now also present another approach that differs from the latter in the way we calculate the FoM. We consider each computational state as an initial state $|\Psi_j\rangle$ on its own and proceed to calculate the time-evolution with Eq. (4.2) where the unitary operator is given by $\tilde{U}_{aim}$ defined in Eq. (4.10). By doing so, we obtain 8 final states $|\Psi_{j,aim}\rangle$:

$$|\Psi_j\rangle \xrightarrow{\text{ccp gate}} |\Psi_{j,aim}\rangle\,, \quad \text{j} = 1,...,8 \tag{4.12}$$

Since the FoM has to quantify the distance between the target state $|\Psi_{j,T}\rangle$ and the final state $|\Psi_{j,aim}\rangle$ we decide to calculate the actual distance between the two states. We do that for all 8 final states and sum the distances together obtaining:

$$FoM = \sum_{j=1}^{8} \| \, |\Psi_{j,aim}\rangle - |\Psi_{j,T}\rangle \, \|^2 \tag{4.13}$$

By examining this procedure more in depth, we comprehend that the FoM defined in Eq. (4.13) is the same FoM given by defining a specific matrix distance between the operators $\tilde{U}_{CPP}$ and $\tilde{U}_{aim}$ defined in Eq. (4.10).

To show this, let us now introduce a specific matrix norm called the Frobenius Norm [34]. Given an operator A, the norm can be defined in the following equivalent ways:

$$\|A\|_F^2 = \sum_{i}^{n} \sum_{j}^{m} |a_{ij}|^2 = \mathrm{Tr}\left[A^\dagger A\right] \tag{4.14}$$

Where n,m denote the number of rows and columns of the matrix. This norm induces a distance, known as Frobenius Distance. Given two operators A_1 and A_2, the distance is defined as the Frobenius norm of a matrix B equal to the difference of the two matrices: $B = A_2 - A_1$.

Let us now calculate the FoM as the Frobenius distance between the operators $\tilde{U}_{CPP} = \tilde{U}^T$ (the c-c-phase gate is the target operator) and $\tilde{U}^{aim}$:

$$FoM_2 = \sum_{i}^{n} \sum_{j}^{m} |\tilde{U}_{ij}^{aim} - \tilde{U}_{ij}^{T}|^2 \tag{4.15}$$

We can now demonstrate that the Figures of Merit defined in Eq. (4.13) and in Eq. (4.15) are the same FoM. Indeed, if we think of the gates as matrices and the states as vectors (columns), we see that the j-th initial state, let us say the second (j = 2), is equal to $|\Psi_2\rangle = |001\rangle = \begin{pmatrix}0 & 1 & 0 & 0 & 0 & 0 & 0 & 0\end{pmatrix}^T$ where in the last notation it is written as a vector in the B basis. Therefore, if we define the columns of $\tilde{U}^{aim}$ as $(\upsilon_1, .., \upsilon_8)$, once we apply the time-evolution operator $\tilde{U}^{aim}$ to the initial state $|\Psi_2\rangle$ in matrix notation, we obtain a final state given by the column υ_2, which therefore has to be equal to $|\Psi_{2,aim}\rangle$. Thus, by doing so for each initial state, we see that the 8 final states match the 8 columns of the time-evolution operator and we can now convince ourselves that the distance between the j-th

target state and the j-th optimization target is equal to the matrix distance between the j-th column of the time-evolution operator and the j-th one of the c-c-phase gate operator. Finally by summing the distances for j going from 1 to 8 we finally get that $FoM_1 = FoM_2 = FoM$.

Having now built the "get_FoM" function with FoM given by Eq. (4.15), we can build the Optimization algorithm following the steps neatly explained in the QuOCS GitHub website, for more details see [18].

4.3.2 Optimization Settings

Now, we define all the parameters of the optimization problem, by collecting them in a particular "json" file named "optimization dictionary". For instance, in this file we define what direct-search method we want to use, the number of bits corresponding to the time grid and so on[5]. Let us now display the main settings of the json file in our case:

- Algorithms: dCRAB and Nelder-Mead direct-search method, or also CMA-ES, both mentioned in Section 4.1. In our case, the preferred direct-search method was NelderMead, but also CMA-ES was used.
- Maximum number of function evaluations (in total) to perform and number of super-iterations was set variably during the analysis.
- Basis selected: the Fourier basis, considering 3 or 4 elements of the basis to build the pulses. Upper limit set to 3. The upper limit quantifies the variability of the pulse, e.g. the higher the upper limit, the greater the number of oscillations, thus higher the frequency. During the analysis these number were changed several times: the ones of basis vectors ranging from 2 to 10, whereas the upper limit from 2 to 8.
- FoM goal, set to 0.00001
- Maximum and minimum values of the pulses respectively set to 2 and -2, and the number of bins to the maximum value set to 101. The interaction strength V is set to 60.
- Inital guess of the pulse set in different ways during the analysis.
- Duration of the gate set to 15.

In particular, the following starting settings have been set for the pulses in the various attempts made:

1. setting the initial pulses to be triangular, in analogy with Ref. [10]. This case was soon discarded since the FoM obtained were very high and much more computational time was needed for them to reach values comparable with other initial guesses, such as the FoM obtained by setting the initial pulse to a constant.
2. setting the initial pulses to the sine function: $\sin\left(\frac{2\pi}{\tau}t\right)$
3. setting the initial pulses to zero and to a constant pulse

4.4 Results

Many attempts were made before reaching an acceptable optimization. Let us overview some of the choices made that consequently lead us to efficiently minimizing the FoM.

First of all, we fix all of the parameters except for Ω_{1r}, as theorically predicted in Section 3.4. Unluckily, this assumption does not lead to an efficient minimization of the FoM. In this case, by setting 6 super-iterations and 20000 maximum function evaluations we obtain the following results:

[5] to see the complete setting of the json file, see Json Settings

By setting the initial pulse to be constant (set to 1), a FoM equal to 6 is reached. By setting it to zero we reach FoM = 7. By setting it to a sine function we obtain FoM = 7.2.

Thus, we decide to perform the optimization with more than one pulse, attempting for example to optimize all 4 pulses. In this case, by setting the initial guesses to zero we obtain FoM = 4, whereas with initial guesses equal to the sine function for all 4 pulses we obtain FoM = 1.3. Being these values better than the previous ones with the single pulse, we assume to be proceeding in the right direction. Then, after several attempts, we find that the winning combination is given by optimizing all 4 parameters and setting each initial pulse differently, thus achieving the FoM goal, FoM $= 9.4 \cdot 10^{-6}$.

Parameter pulses	**Initial Guesses**	**Basis Vectors**
Ω_{01}	constant = 0	3
Ω_{1r}	sine function	4
Δ_{01}	constant = 0.1	3
Δ_{1r}	sine function	4

Table 4.1: *Winning combination of initial guesses and number of basis vectors with respect to the parameter pulses to achieve FoM goal of* 10^{-5}

We now want to conclude by comparing $\tilde{U}_T = \tilde{U}_{CCP}$ with $\tilde{U}_{aim}$ which corresponds to the optimized time-evolution operator:

ŨCPP

$$\begin{pmatrix}
1 & 0 & 0 & 0 & 0 & 0 & 0 & 0 \\
0 & 1 & 0 & 0 & 0 & 0 & 0 & 0 \\
0 & 0 & 0 & 0 & 0 & 0 & 0 & 0 \\
0 & 0 & 1 & 0 & 0 & 0 & 0 & 0 \\
0 & 0 & 0 & 1 & 0 & 0 & 0 & 0 \\
0 & 0 & 0 & 0 & 0 & 0 & 0 & 0 \\
0 & 0 & 0 & 0 & 0 & 0 & 0 & 0 \\
0 & 0 & 0 & 0 & 0 & 0 & 0 & 0 \\
0 & 0 & 0 & 0 & 0 & 0 & 0 & 0 \\
0 & 0 & 0 & 0 & 1 & 0 & 0 & 0 \\
0 & 0 & 0 & 0 & 0 & 1 & 0 & 0 \\
0 & 0 & 0 & 0 & 0 & 0 & 0 & 0 \\
0 & 0 & 0 & 0 & 0 & 0 & 1 & 0 \\
0 & 0 & 0 & 0 & 0 & 0 & 0 & -1 \\
0 & 0 & 0 & 0 & 0 & 0 & 0 & 0 \\
0 & 0 & 0 & 0 & 0 & 0 & 0 & 0 \\
0 & 0 & 0 & 0 & 0 & 0 & 0 & 0 \\
0 & 0 & 0 & 0 & 0 & 0 & 0 & 0 \\
0 & 0 & 0 & 0 & 0 & 0 & 0 & 0 \\
0 & 0 & 0 & 0 & 0 & 0 & 0 & 0 \\
0 & 0 & 0 & 0 & 0 & 0 & 0 & 0 \\
0 & 0 & 0 & 0 & 0 & 0 & 0 & 0 \\
0 & 0 & 0 & 0 & 0 & 0 & 0 & 0 \\
0 & 0 & 0 & 0 & 0 & 0 & 0 & 0 \\
0 & 0 & 0 & 0 & 0 & 0 & 0 & 0 \\
0 & 0 & 0 & 0 & 0 & 0 & 0 & 0 \\
0 & 0 & 0 & 0 & 0 & 0 & 0 & 0
\end{pmatrix}$$

UAIM

$$\begin{pmatrix}
1.00000 & -0.00000 & -0.00000 & -0.00000 & -0.00000 & -0.00000 & -0.00000 & 0.00000 \\
-0.00000 & 1.00000 & -0.00000 & -0.00000 & -0.00000 & -0.00000 & 0.00000 & -0.00000 \\
-0.00000 & -0.00000 & 0.00000 & -0.00000 & 0.00000 & -0.00000 & 0.00000 & 0.00000 \\
-0.00000 & -0.00000 & 1.00000 & -0.00000 & -0.00000 & 0.00000 & -0.00000 & -0.00000 \\
-0.00000 & -0.00000 & -0.00000 & 1.00000 & -0.00000 & 0.00000 & 0.00000 & 0.00000 \\
-0.00000 & 0.00000 & -0.00000 & 0.00000 & -0.00000 & -0.00000 & -0.00000 & 0.00000 \\
-0.00000 & 0.00000 & -0.00000 & -0.00000 & 0.00000 & 0.00000 & -0.00000 & 0.00000 \\
-0.00000 & -0.00000 & 0.00000 & 0.00000 & -0.00000 & -0.00000 & -0.00000 & 0.00000 \\
0.00000 & -0.00000 & -0.00000 & -0.00100 & 0.00000 & 0.00000 & 0.00000 & -0.00000 \\
-0.00000 & -0.00000 & -0.00000 & 0.00000 & 1.00000 & -0.00000 & -0.00000 & -0.00000 \\
-0.00000 & -0.00000 & -0.00000 & 0.00000 & -0.00000 & 1.00000 & 0.00000 & 0.00000 \\
-0.00000 & 0.00000 & -0.00000 & -0.00000 & -0.00000 & 0.00000 & -0.00000 & 0.00000 \\
-0.00000 & -0.00000 & -0.00000 & 0.00000 & -0.00000 & 0.00000 & 1.00000 & 0.00000 \\
0.00000 & -0.00000 & -0.00000 & -0.00000 & -0.00000 & -0.00000 & -0.00000 & -1.00000 \\
-0.00000 & 0.00000 & -0.00000 & 0.00000 & -0.00000 & 0.00000 & -0.00000 & 0.00000 \\
-0.00000 & -0.00000 & 0.00000 & -0.00000 & -0.00000 & -0.00000 & 0.00000 & 0.00000 \\
-0.00000 & -0.00000 & 0.00000 & 0.00000 & -0.00000 & -0.00000 & 0.00000 & 0.00000 \\
0.00000 & -0.00000 & -0.00000 & -0.00000 & 0.00000 & 0.00000 & 0.00000 & 0.00100 \\
-0.00000 & 0.00000 & 0.00000 & 0.00000 & -0.00000 & -0.00000 & -0.00000 & 0.00000 \\
-0.00000 & -0.00000 & -0.00000 & -0.00000 & 0.00000 & 0.00000 & -0.00000 & 0.00000 \\
0.00000 & -0.00000 & 0.00000 & 0.00000 & -0.00000 & -0.00100 & 0.00000 & -0.00000 \\
-0.00000 & -0.00000 & -0.00000 & -0.00000 & 0.00000 & -0.00000 & 0.00000 & 0.00000 \\
-0.00000 & -0.00000 & -0.00000 & -0.00000 & 0.00000 & 0.00000 & 0.00000 & 0.00000 \\
0.00000 & -0.00000 & 0.00000 & 0.00000 & -0.00000 & -0.00000 & 0.00000 & 0.00100 \\
0.00000 & 0.00000 & -0.00000 & 0.00000 & -0.00000 & 0.00000 & -0.00100 & -0.00000 \\
0.00000 & 0.00000 & -0.00000 & 0.00000 & -0.00000 & 0.00000 & -0.00000 & 0.00100 \\
-0.00000 & -0.00000 & -0.00000 & 0.00000 & -0.00000 & 0.00000 & 0.00000 & -0.00000
\end{pmatrix}$$

Figure 4.1: *Comparison between* $\tilde{U}_{CCP}$ *with* $\tilde{U}_{aim}$*. Components of* U_{aim} *rounded to the third decimal digit.*

We observe that the two gates are almost identical. Therefore, we can confidently state that the optimization has been successfully achieved: we have found the parameter pulses that realize the controlled-controlled-phase gate.

Finally, we display here the pulses obtained by two separate optimizations, starting from the same combination displayed in Table 4.1, both achieving the FoM goal:

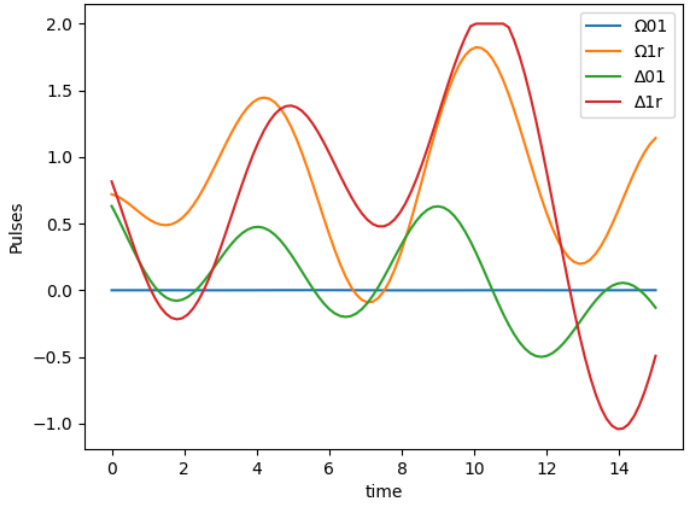

(a)

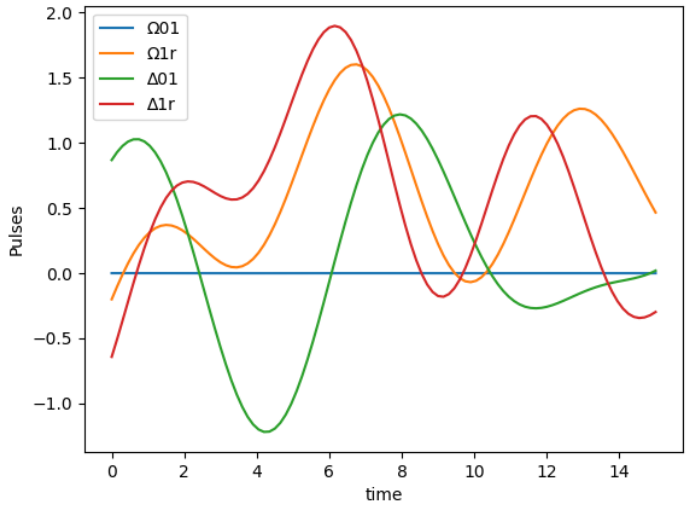

(b)

Figure 4.2: *Optimized Paramater Pulses for the realization of the c-c-phase gate (a) Optimized Pulses with FoM equal to* 10^{-5}*. (b) Optimized Pulses with FoM equal to* $9.4 \cdot 10^{-6}$

Chapter 5

Conclusion

In this Thesis we have focused on the quantum optimization of a particular three-qubit gate named controlled-controlled-phase gate.

We initially analyzed the main features of Rydberg atoms, especially focusing on the Rydberg Blockade phenomenon, acknowledging its crucial role for entangling gates. We later observed how it introduces entanglement by examining the case of the two-qubit controlled-phase gate, where we have concluded that different trajectories traced by initial states $|01\rangle$ and $|11\rangle$, are to be attributed to the Rydberg blockade effect. The different trajectories then lead the initial states to acquire different phases and by satisfying the relation in Eq. (2.14) we implement the controlled-phase. In addition, the Hamiltonian of the controlled-phase gate supplied us with the the tools to generalize the system to a three-qubit gate.

We then observed that the symmetry of the c-c-phase gate translates into a specific geometry of the setup where the Rydberg atoms are placed in an equilateral triangle. Furthermore, by performing the testing in Chapter 3, we found that the Lie Algebra of the Hamiltonian does not match with the vector-space of permutation-invariant operators. We also figured out a general way to generate a Hermitian Lie Algebra starting from the Hermitian generators of the Hamiltonian.

In the second testing phase we have discovered a new approach that can be adopted for the implementation of a multi-qubit gate, that is the restriction of gate to the logical basis where we only we consider the computational states by excluding the Rydberg state $|r\rangle$, which corresponds to filtering the gate's action to the states we can actually measure and manipulate for quantum computation. Therefore, by rearranging the columns of the gate, we only need to require that the gate has the form of the block matrix defined in Eq. (3.15), and since the Lie Algebra is Hermitian, we can impose this by filtering the Lie Algebra to the logical basis and checking if the filtered generator is contained in the filtered Lie Algebra. In this way, we found the first remarkable result of the project, namely that the filtered c-c-phase gate can be achieved at least from a theoretical point of view by our Rydberg Setup.

Moreover, two important aspects emerged from the third check. On one hand, we can still obtain the c-c-phase gate by neglecting three parameters in the dynamics of the system, which are: the detunings Δ_{01}, Δ_{1r} and the Rabi frequency Ω_{01}. On the other hand, it is impossible to obtain an entangling gate without considering the dipole-dipole interaction between the Rydberg states, confirming what previously stated in examining the Rydberg Blockade.

In conclusion, we explored a generic Quantum Optimal Control problem to fully comprehend how to apply it to our specific case. We then learned how to transform the optimization of several pulse shapes into a minimization problem of a functional, and how to solve it by applying the dCRAB algorithm. Moreover, we figured out the right way to write the functional (Figure of Merit) of the problem, by introducing the Frobenius Distance and finally, after several attempts, neglecting the decoherence time error, we accomplished the minimization of the Figure of Merit with $FoM = 10^{-5}$, successfully optimizing the parameter pulses. We also found out that, differently from what theoretically predicted in Section 3.4, it is incredibly difficult to optimize the laser pulse by only varying the Rabi frequency Ω_{01}. Therefore, even though the other parameters are negligible in theory, they are almost essential for the actual optimization of the controlled-controlled-phase gate.

Bibliography

[1] Richard P. Feynman. "Simulating physics with computers". In: *International Journal of Theoretical Physics* 21.6 (June 1982), pp. 467–488. ISSN: 1572-9575. DOI: 10.1007/BF02650179. URL: https://doi.org/10.1007/BF02650179.

[2] David S Weiss and Mark Saffman. "Quantum computing with neutral atoms". In: *Phys. Today* 70.7 (July 2017), pp. 44–50.

[3] Frank Arute et al. "Quantum supremacy using a programmable superconducting processor". In: *Nature* 574.7779 (2019), pp. 505–510. DOI: 10.1038/s41586-019-1666-5.

[4] Vasileios Mavroeidis et al. "The Impact of Quantum Computing on Present Cryptography". In: *International Journal of Advanced Computer Science and Applications* 9.3 (2018). DOI: 10.14569/ijacsa.2018.090354. URL: https://doi.org/10.14569%5C%2Fijacsa.2018.090354.

[5] Adam Smith et al. "Simulating quantum many-body dynamics on a current digital quantum computer". In: *npj Quantum Information* 5.1 (Nov. 2019), p. 106. ISSN: 2056-6387. DOI: 10.1038/s41534-019-0217-0. URL: https://doi.org/10.1038/s41534-019-0217-0.

[6] He-Liang Huang et al. "Superconducting quantum computing: a review". In: *Science China Information Sciences* 63.8 (July 2020). DOI: 10.1007/s11432-020-2881-9. URL: https://doi.org/10.1007%2Fs11432-020-2881-9.

[7] Colin D. Bruzewicz et al. "Trapped-ion quantum computing: Progress and challenges". In: *Applied Physics Reviews* 6.2 (June 2019), p. 021314. DOI: 10.1063/1.5088164. URL: https://doi.org/10.1063/1.5088164.

[8] Alice Pagano. "Optimal quantum gates for Rydberg atoms quantum computer". In: *Master thesis* (2021). URL: https://thesis.unipd.it/browse?type=author&authority=st766495.

[9] D. Jaksch et al. "Fast Quantum Gates for Neutral Atoms". In: *Phys. Rev. Lett.* 85 (10 Sept. 2000), pp. 2208–2211. DOI: 10.1103/PhysRevLett.85.2208. URL: https://link.aps.org/doi/10.1103/PhysRevLett.85.2208.

[10] Alice Pagano et al. "Error budgeting for a controlled-phase gate with strontium-88 Rydberg atoms". In: *Phys. Rev. Res.* 4 (3 July 2022), p. 033019. DOI: 10.1103/PhysRevResearch.4.033019. URL: https://link.aps.org/doi/10.1103/PhysRevResearch.4.033019.

[11] E. Urban et al. "Observation of Rydberg blockade between two atoms". In: *Nature Physics* 5.2 (Feb. 2009), pp. 110–114. ISSN: 1745-2481. DOI: 10.1038/nphys1178. URL: https://doi.org/10.1038/nphys1178.

[12] Alpha Gaëtan et al. "Observation of collective excitation of two individual atoms in the Rydberg blockade regime". In: *Nature Physics* 5.2 (Feb. 2009), pp. 115–118. ISSN: 1745-2481. DOI: 10.1038/nphys1183. URL: https://doi.org/10.1038/nphys1183.

[13] Ivaylo S. Madjarov et al. "High-fidelity entanglement and detection of alkaline-earth Rydberg atoms". In: *Nature Physics* 16.8 (Aug. 2020), pp. 857–861. ISSN: 1745-2481. DOI: 10.1038/s41567-020-0903-z. URL: https://doi.org/10.1038/s41567-020-0903-z.

[14] I. I. Beterov et al. "Fast three-qubit Toffoli quantum gate based on three-body Förster resonances in Rydberg atoms". In: *Phys. Rev. A* 98 (4 Oct. 2018), p. 042704. DOI: 10.1103/PhysRevA.98.042704. URL: https://link.aps.org/doi/10.1103/PhysRevA.98.042704.

[15] Yaoyun Shi. *Both Toffoli and Controlled-NOT need little help to do universal quantum computation*. 2002. DOI: 10.48550/ARXIV.QUANT-PH/0205115. URL: https://arxiv.org/abs/quant-ph/0205115.

[16] D. G. Cory et al. "Experimental Quantum Error Correction". In: *Physical Review Letters* 81.10 (Sept. 1998), pp. 2152–2155. DOI: 10.1103/physrevlett.81.2152. URL: https://doi.org/10.1103%5C%2Fphysrevlett.81.2152.

[17] Takao Aoki et al. "Quantum error correction beyond qubits". In: *Nature Physics* 5.8 (Aug. 2009), pp. 541–546. ISSN: 1745-2481. DOI: 10.1038/nphys1309. URL: https://doi.org/10.1038/nphys1309.

[18] Marco Rossignolo et al. *QuOCS: The Quantum Optimal Control Suite*. 2022. DOI: 10.48550/ARXIV.2212.11144. URL: https://arxiv.org/abs/2212.11144.

[19] Xiaoling Wu et al. "A concise review of Rydberg atom based quantum computation and quantum simulation∗". In: *Chinese Physics B* 30.2 (Feb. 2021), p. 020305. DOI: 10.1088/1674-1056/abd76f. URL: https://doi.org/10.1088%5C%2F1674-1056%5C%2Fabd76f.

[20] Sebastian Weber et al. "Calculation of Rydberg interaction potentials". In: *Journal of Physics B: Atomic, Molecular and Optical Physics* 50.13 (June 2017), p. 133001. DOI: 10.1088/1361-6455/aa743a. URL: https://doi.org/10.1088%5C%2F1361-6455%5C%2Faa743a.

[21] J.M. Nipper and T. Pfau. *Interacting Rydberg Atoms: Coherent Control at Förster Resonances and Polar Homonuclear Molecules*. 2012.

[22] Jianmin Tao, John P. Perdew, and Adrienn Ruzsinszky. "Accurate van der Waals coefficients from density functional theory". In: *Proceedings of the National Academy of Sciences* 109.1 (2012), pp. 18–21. DOI: 10.1073/pnas.1118245108. eprint: https://www.pnas.org/doi/pdf/10.1073/pnas.1118245108. URL: https://www.pnas.org/doi/abs/10.1073/pnas.1118245108.

[23] Christopher J. Foot. *Atomic Physics*. New York, NY: Oxford University Press, 2005.

[24] Michael A. Nielsen and Isaac L. Chuang. *Quantum Computation and Quantum Information: 10th Anniversary Edition*. Cambridge University Press, 2010. DOI: 10.1017/CBO9780511976667.

[25] J. J. Sakurai and Jim Napolitano. *Modern Quantum Mechanics*. Cambridge University Press, Sept. 2017. DOI: 10.1017/9781108499996. URL: https://doi.org/10.1017/9781108499996.

[26] Fritz Riehle. *Frequency Standards: Basics and Applications*. John Wiley & Sons, 2006.

[27] Yehuda B. Band and Yshai Avishai. "5 - Quantum Information". In: *Quantum Mechanics with Applications to Nanotechnology and Information Science*. Ed. by Yehuda B. Band and Yshai Avishai. Amsterdam: Academic Press, 2013, pp. 193–258. ISBN: 978-0-444-53786-7. DOI: https://doi.org/10.1016/B978-0-444-53786-7.00005-8. URL: https://www.sciencedirect.com/science/article/pii/B9780444537867000058.

[28] Tommaso Toffoli. "Reversible computing". In: *Automata, Languages and Programming*. Ed. by Jaco de Bakker and Jan van Leeuwen. Berlin, Heidelberg: Springer Berlin Heidelberg, 1980, pp. 632–644. ISBN: 978-3-540-39346-7.

[29] Peter W. Shor. "Polynomial-Time Algorithms for Prime Factorization and Discrete Logarithms on a Quantum Computer". In: *SIAM Review* 41.2 (1999), pp. 303–332. DOI: 10.1137/S0036144598347011. eprint: https://doi.org/10.1137/S0036144598347011. URL: https://doi.org/10.1137/S0036144598347011.

[30] Michael A. Nielsen and Isaac Chuang. "Quantum Computation and Quantum Information". In: *American Journal of Physics* 70.5 (2002), pp. 558–559. DOI: 10.1119/1.1463744. eprint: https://doi.org/10.1119/1.1463744. URL: https://doi.org/10.1119/1.1463744.

[31] T. Monz et al. "Realization of the Quantum Toffoli Gate with Trapped Ions". In: *Phys. Rev. Lett.* 102 (4 Jan. 2009), p. 040501. DOI: 10.1103/PhysRevLett.102.040501. URL: https://link.aps.org/doi/10.1103/PhysRevLett.102.040501.

[32] A. Fedorov et al. "Implementation of a Toffoli gate with superconducting circuits". In: *Nature* 481.7380 (Dec. 2011), pp. 170–172. DOI: 10.1038/nature10713. URL: https://doi.org/10.1038%5C%2Fnature10713.

[33] M. D. Reed et al. "Realization of three-qubit quantum error correction with superconducting circuits". In: *Nature* 482.7385 (Feb. 2012), pp. 382–385. DOI: 10.1038/nature10786. URL: https://doi.org/10.1038%5C%2Fnature10786.

[34] Roger A. Horn and Charles R. Johnson. *Topics in Matrix Analysis (2nd ed.)* Cambridge: Cambridge University Press, 1985.

[35] Arnold Neumaier and Dennis Westra. *Classical and Quantum Mechanics via Lie algebras*. 2008. DOI: 10.48550/ARXIV.0810.1019. URL: https://arxiv.org/abs/0810.1019.

[36] J. Werschnik and E. K. U. Gross. *Quantum Optimal Control Theory*. 2007. DOI: 10.48550/ARXIV.0707.1883. URL: https://arxiv.org/abs/0707.1883.

[37] S. Machnes et al. "Comparing, optimizing, and benchmarking quantum-control algorithms in a unifying programming framework". In: *Phys. Rev. A* 84 (2 Aug. 2011), p. 022305. DOI: 10.1103/PhysRevA.84.022305. URL: https://link.aps.org/doi/10.1103/PhysRevA.84.022305.

[38] Tommaso Caneva, Tommaso Calarco, and Simone Montangero. "Chopped random-basis quantum optimization". In: *Phys. Rev. A* 84 (2 Aug. 2011), p. 022326. DOI: 10.1103/PhysRevA.84.022326. URL: https://link.aps.org/doi/10.1103/PhysRevA.84.022326.

[39] Matthias M Müller et al. "One decade of quantum optimal control in the chopped random basis". In: *Reports on Progress in Physics* 85.7 (June 2022), p. 076001. DOI: 10.1088/1361-6633/ac723c. URL: https://doi.org/10.1088%5C%2F1361-6633%5C%2Fac723c.

[40] Phila Rembold et al. "Introduction to quantum optimal control for quantum sensing with nitrogen-vacancy centers in diamond". In: *AVS Quantum Science* 2.2 (June 2020), p. 024701. DOI: 10.1116/5.0006785. URL: https://doi.org/10.1116%5C%2F5.0006785.